

EFFECT OF AUSFORMING VIA SEVERE PLASTIC DEFORMATION
ON SHAPE MEMORY BEHAVIOR OF NiTi

A Thesis

by

AJAY V KULKARNI

Submitted to the Office of Graduate Studies of
Texas A&M University
in partial fulfillment of the requirements for the degree of

MASTER OF SCIENCE

December 2004

Major Subject: Mechanical Engineering

EFFECT OF AUSFORMING VIA SEVERE PLASTIC DEFORMATION
ON SHAPE MEMORY BEHAVIOR OF NiTi

A Thesis

by

AJAY V KULKARNI

Submitted to Texas A&M University
in partial fulfillment of the requirements
for the degree of

MASTER OF SCIENCE

Approved as to style and content by:

Ibrahim Karaman
(Chair of Committee)

Richard Griffin
(Member)

Amy Epps Martin
(Member)

Dennis L. O'Neal
(Head of Department)

December 2004

Major Subject: Mechanical Engineering

ABSTRACT

Effect of Ausforming via Severe Plastic Deformation on Shape Memory Behavior of NiTi. (December 2004)

Ajay V Kulkarni, B.S., Pune University

Chair of Advisory Committee: Dr. Ibrahim Karaman

In this study, thermomechanical properties of Ti-50.8 and 50.7 at% Ni alloy severely deformed using Equal Channel Angular Extrusion (ECAE) are investigated. The aim of this study is to reveal the effects of severe plastic deformation on shape memory, pseudelasticity, interplay between plastic deformation via dislocation slip and twinning, and forward and reverse martensitic transformation. The samples are processed at room temperature, i.e. slightly above the austenite finish temperature, and at 450 °C, i.e. well-above the austenite finish temperature. Transformation temperatures, microstructural evolution, and thermomechanical properties of ECAE processed samples are studied before and after low temperature annealing heat treatment and compared with conventional cold drawn and precipitation hardened material. The unique findings are: 1) the observation of a mixture of heavily deformed B2 (austenite) and B19' (martensite) phases in the samples processed at room temperature although martensite stabilization was expected, 2) the observation of highly organized, twin-related nanograins in B2 phase of the samples deformed at room temperature which was attributed to $B2 \xrightarrow{\text{SIM}} B19' \xrightarrow{\text{SPD}} B2$ (SIM: Stress Induced Martensitic transformation, SPD: Severe Plastic Deformation) transformation sequence, 3) simultaneous observation of B2 austenite and strain induced B19' martensite in the samples deformed at 450 °C, and 4) perfect pseudoelasticity, small pseudoelastic stress hysteresis and excellent cyclic response with no irrecoverable strain up to 1000 cycles for ECAE at 450 °C processed

sample. Strain induced martensite in NiTi alloys was reported for the first time. The formation of well-organized twin-related nanograins via severe plastic deformation opens a new opportunity for twinning induced grain boundary engineering in NiTi alloys which significantly improves the matrix strength and the cyclic response against degradation of shape memory and pseudoelasticity.

To My Parents

ACKNOWLEDGEMENTS

First of all, I sincerely thank my advisor, Prof. Ibrahim Karaman, for being supportive and understanding right from the beginning; he inspired and motivated me by being a role model for me. He not only helped me in every aspect of this project but also made me a better person, scientist, and engineer by setting high standards.

I am thankful to Prof. Richard Griffin and Prof. Amy Epps Martin, for being my committee members.

I express my gratitude to Prof. Yuriy Chumlyakov for his invaluable suggestions and guidelines in my research and for sharing with me his deep knowledge on shape memory alloys. Discussions with him have always been a pleasure for me.

I am also grateful to Dr. Zhiping Luo, who helped me in TEM and indexing of the diffraction patterns, to Robert Barber for performing the extrusions and giving invaluable inputs in day to day problems, and to Bill Merka from the chemistry glass shop for encapsulating the samples for heat treatment.

Special thanks to my officemates: Anish Simon, Haluk Karaca, Joesph Mather, Bryan Bagley, Guney Yapici, Mohammed Haouaoui, Benat Kockar, Burak Basaran, Yang Cao and Suveen Mathandu for being helpful and for providing a good environment for research and their social relations. Special thanks to Anish Simon for being such a good friend. Thanks to Haluk Karaca, Guney Yapici, Burak Basaran and Dr.Karaman for teaching me a lot about their Turkish cultures and to Haluk Karaca who gave me chance to taste delicious Turkish food.

I also thank all my friends: Shantur Tapar, Hemendra Khakhar, Rahul Joshi, Prasad Garimella, Suhas Verma, Amit Goel, Ajit Ambike, Ruchir Patwa, Yash Shukla, Shabib Kadri, Chirag Shah, Tapan Kulkarni and many others in College Station for helping me adopt a new life style and enjoy my life and not letting me feel secluded from my Home Country and family.

Finally, I thank my parents who have always trusted and inspired me for my future endeavors. They have undertaken and overcome lots of difficulties in educating me and making me a better person. I would also like to thank my relatives back in India Karhadkar, Damodare, Dharmadhikari family who have endowed me with their blessings.

TABLE OF CONTENTS

	Page
ABSTRACT	iii
DEDICATION	v
ACKNOWLEDGEMENTS	vi
TABLE OF CONTENTS.....	viii
LIST OF FIGURES	x
LIST OF TABLES	xiv
CHAPTER	
I INTRODUCTION.....	1
1.1 Background.....	1
1.2 Brief history of SMAs	6
1.3 Phase diagrams	8
1.4 Crystal structures	9
1.5 Self accommodation	12
1.6 Ductility of NiTi.....	14
1.7 Determination of transformation temperatures	15
II MOTIVATION.....	17
III EXPERIMENTAL PROCEDURE.....	21
3.1 Extrusions	21
3.2 Calorimetric analysis	23
3.3 Microstructural evolution	23
3.4 Thermomechanical testing.....	23
IV RESULTS AND DISCUSSION.....	27
4.1 Calorimetric analysis	27
4.2 Microstructural evolution after ECAE processing	35
4.3 Microstructural observation in annealed material after ECAE processing	43

	Page
CHAPTER	
4.4 Mechanical properties	52
a. Incremental straining	52
b. Thermal cycling response under stress.....	58
c. Pseudoelastic cyclic response.....	67
d. Effect of ECAE on ductility	71
V CONCLUSION AND FUTURE RECOMMENDATION.....	74
REFERENCES.....	76
VITA.....	78

LIST OF FIGURES

	Page
Figure 1.1.1 The deformation of a sphere into an ellipsoid and the definition of K_1 , η_1 , K_2 and η_2	2
Figure 1.1.2 Basic self-accommodating morphologies.....	3
Figure 1.1.3 Electric resistance vs. temperature curves for thermoelastic and nonthermoelastic shape memory alloys.....	4
Figure 1.1.4 A schematic of stress-strain behavior of shape memory alloys.....	7
Figure 1.3.1 Phase diagram of NiTi	9
Figure 1.4.1 Structural relationship among cubic parent phase (B2) and two kinds of martensites B19 and B19', (a) the parent phase B2, (b) orthorhombic martensite B19, (c) monoclinic B19' martensite of NiTi.....	11
Figure 1.5.1 Self accommodating morphology of B19'	12
Figure 1.5.2 Self accommodating morphology of R phase.....	13
Figure 1.5.3 Self accommodating morphology of B19 phase.....	14
Figure 1.7.1. Schematic of intersecting slope method for finding transformation temperatures from DSC response.	16
Figure 2.1 Schematic representation of ECAE process	20
Figure 3.1.1 250 ton extrusion press at Texas A&M University	22
Figure 3.4.1 Servohydraulic MTS test frame used for thermomechanical testing.....	25
Figure 3.4.2 Miniature Materials Test Systems (MTS) extensometer with a 3 mm gage length	26
Figure 4.1.1 DSC response of as-received, solutionized and ECAE processed material.	28
Figure 4.1.2 DSC response of the material solutionized and aged at 450 °C for 1 hour showing a three stage martensitic transformation, i.e. austenite to R-phase transformation, R-phase to martensite transformation near precipitates (M^P), and R-phase to martensite transformation away from precipitates (M^M)......	29
Figure 4.1.3 Effect of annealing temperature on the transformation behavior of ECAE processed material (a) DSC response of ECAE at RT, (b) DSC response of ECAE at 450 °C, (c) TTs for ECAE at RT, and (d) TTs for ECAE at 450 °C samples. TTs of the solutionized and	

	Page
	31
Figure 4.2.1	37
Figure 4.2.2	38
Figure 4.2.3	39
Figure 4.2.4	39
Figure 4.2.5	41
Figure 4.2.6	42
Figure 4.3.1	44
Figure 4.3.2	

	Page
circled area marked as “c” in Fig. (a). The EDP in Fig. (d) is taken from the circle marked as “d” in Fig. (a), showing the reflections of both matrix and twins. Note there is a secondary plane trace with angle of 16° apart away from $(2\ 1\ -1)$, which is identified as $(4\ 1\ -1)$ which trace is perpendicular to the $g(4\ 1\ -1)$ vector.....	45
Figure 4.3.3 Bright field TEM images of ECAE at RT material after annealing at $600\ ^\circ\text{C}$ for 30 minutes	46
Figure 4.3.4 Bright field TEM images of ECAE at RT material after annealing at $700\ ^\circ\text{C}$ for 30 minutes	47
Figure 4.3.5 Effect of annealing temperature on the grain size of ECAE at RT material	48
Figure 4.3.6 Effect of grain size on temperature hysteresis for the ECAE at RT material after different annealing treatments	49
Figure 4.3.7 Optical micrograph of 50.7 at % NiTi after (a) ECAE at $450\ ^\circ\text{C}$ 1A route, and (b) ECAE at $450\ ^\circ\text{C}$ 2C route.	50
Figure 4.4.1.a Incremental strain response under compression of as-received material	53
Figure 4.4.1.b Incremental strain response under compression of solutionized material	54
Figure 4.4.1.c Incremental strain response under compression of as received + annealed at 450°C for 1hr. material	55
Figure 4.4.1.d Incremental strain response under compression of solutionized + aged at 450°C for 1hr material	56
Figure 4.4.1.e Incremental strain response under compression of ECAE at 450°C material	57
Figure 4.4.2 Definition of transformation strain and thermal hysteresis on a standard strain - temperature response of SMAs during thermal cycling under stress.....	59
Figure 4.4.3 Strain - Temperature response under thermal cycling at various stress levels for (a) as-received, (b) as-received + annealed at 350°C for 30min, (c) as-received + annealed at 450°C for one hr, (d) solutionized, (e) solutionized + aged at 400°C for 30min, and (f) ECAE processed at 450°C	60
Figure 4.4.4 Variation of transformation strain as a function of applied stress for various deformation and heat treatment conditions	64

	Page
Figure 4.4.5 Stress dependence of thermal hysteresis for various deformation and heat treatment conditions	65
Figure 4.4.6 Variation of irrecoverable strain as a function of applied stress for various deformation and heat treatment conditions	66
Figure 4.4.7 Cyclic response at 3% compressive strain for (a) solutionized, (b) as-received, annealed at 450°C for one hr and (c) ECAE at 450°C	69
Figure 4.4.8 Incremental strain response under tension of 50.7 at % NiTi Hot Rolled material after ECAE at 450°C 1A	73

LIST OF TABLES

	Page
Table 2.1	Some typical SMA applications, underlying SM effects and expected fatigue lives N_f 17
Table 3.1.1	Summary of extrusions 22
Table 4.1.1	Comparison of various parameters pertinent to cyclic response of shape memory alloys for different deformation and heat treatment conditions, SIM: Stress for Inducing Martensite, PE: Pseudoelastic... 71

CHAPTER I

INTRODUCTION

The basic objective of this study is to analyze the effects of ausforming via ECAE as a tool for severe plastic deformation (SPD) on shape memory behaviour of NiTi. Ausforming is the deformation in austenitic state. First an introduction to basic concepts of shape memory alloys (SMAs) is presented followed by experimental procedure including a brief summary of extrusions followed by results and discussion i.e. calorimetric analysis, microstructural evolution, and thermomechanical testing and finally we draw conclusions based on the results and discussion and give some recommendations for future work.

1.1 Background

Shape memory alloys (SMAs) have unique properties, such as high recoverable strains, as a result of reversible, diffusionless martensitic transformation (MT). Phase transformation can be triggered by temperature change, applied stress or magnetic field and a high temperature phase called austenite or parent phase transforms to a low temperature and lower symmetry phase called martensite and vice versa.

MT can be defined simply as a lattice deformation involving shearing deformation and resulting from cooperative atomic movement. There is a 1-to-1 correspondence called “lattice correspondence” between the lattice points of parent and martensitic phases. Habit plane is a specific plane between the parent and martensitic phase along which the shear occurs during transformation. Since there is no strain and rotation in the habit plane throughout the entire transformation, this type of shape deformation is called invariant shear strain. Martensites with different habit planes are called variants [1].

MT is a first order transformation which results in large transformation strain. In order to reduce the strain during nucleation and growth, two types of lattice invariant

This thesis follows the style and format of Acta Materialia.

shear (LIS) mechanisms could take place: dislocation slip or twinning [2]. These are called LIS because they do not change the structure of martensite. Generally twinning is the LIS for most SMAs. A schematic of a twinning system is shown in Figure 1.1.1.

K_1 and η_1 are called the shear plane and shear direction, respectively. K_1 is an invariant plane, and K_2 is another undistorted plane. The plane which is normal to K_1 and parallel to η_1 is called the plane of shear, and η_2 is the intersection of K_2 and the plane of shear. If K_1 and η_2 are rational and K_2 and η_1 are irrational, the twinning is called type I twinning. If K_1 and η_2 are irrational and K_2 and η_1 are rational, the twinning is called type II twinning. If all of them are rational, compound twinning occurs.

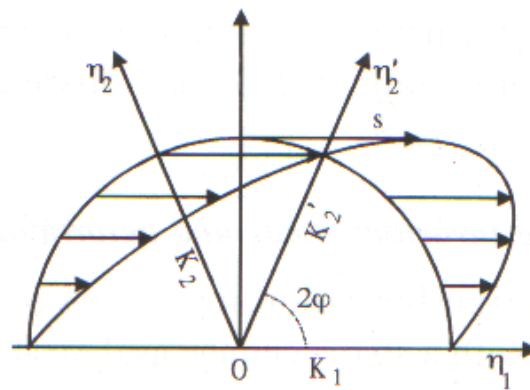


Figure 1.1.1 The deformation of a sphere into an ellipsoid and the definitions of K_1 , η_1 , K_2 and η_2 [2].

The driving force for diffusionless phase transformation in SMAs is the chemical free energy between the phases. When the difference in chemical free energies is enough

to overcome the energy to nucleate the other phase, transformation will start and continue as the energy for growth is supplied by further increase in the chemical energy difference. The transformation start and finish temperatures from austenite to martensite are called M_s and M_f , respectively, and transformation start and finish temperatures from martensite to austenite are called A_s and A_f , respectively, where the former transformation is called a forward transformation and the latter one a back transformation.

When the MT starts during cooling in order to minimize the strain, a second step of strain minimization takes place in addition to LIS which is self accommodation of martensite variants. Martensite variants are created side by side and they mutually reduce the transformation strain accompanying the formation of the martensite variants. This effect is called self-accommodation. Thus the specimen as a whole will not experience any shape change whatsoever. The basic morphologies of self accommodation structures are shown in Figure 1.1.2 and are called diamond and parallelogram morphology of self accommodation. Different self accommodation morphologies could be formed as will be shown later for NiTi alloys.

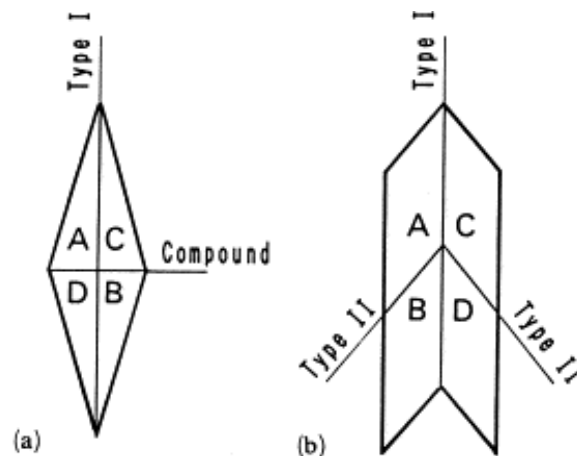


Figure 1.1.2 Basic self-accommodating morphologies [3].

MTs can be classified in two categories: thermoelastic and nonthermoelastic. For thermoelastic MTs, the transformation temperature hysteresis is small, the interface between parent and martensite is mobile, and the transformation is crystallographically reversible. For nonthermoelastic MTs, the transformation temperature hysteresis is large, the interface between the martensite and parent phase is immobile, and once the martensite grows to some critical size, the reverse transformation takes place by renucleation of the parent phase. Figure 1.1.3 shows the difference in transformation temperature hysteresis between the thermoelastic and nonthermoelastic MTs. Most of the thermoelastic shape memory alloys are intermetallic alloys since they have an ordered structure, which means that lattice sites are occupied by a particular species of atoms. Since MT is a diffusionless process, the product martensite is also ordered and the process is crystallographically reversible. Ordering also promotes a higher flow stress in the parent phase which prevents damage of the martensite/parent interphase during growth of martensite.

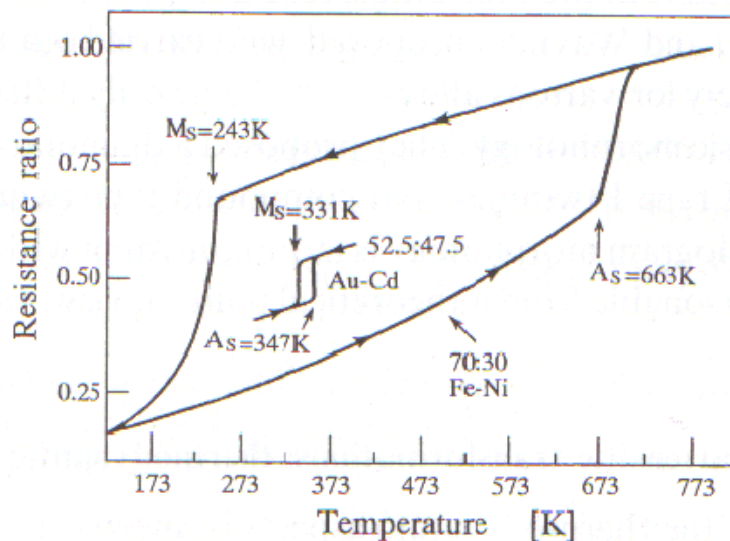


Figure 1.1.3 Electric resistance vs. temperature curves for thermoelastic and nonthermoelastic shape memory alloys [2].

There are two deformation types in shape memory alloys which lead to high recoverable strains: reorientation of martensite and stress induced martensite. When NiTi alloys cool down under zero stress, the parent phase transforms to martensite and 24 possible internally twinned martensite variants form self-accommodating structures to minimize the macroscopic volume change [1]. The applied stress biases the self-accommodating structure and favors the growth of selected martensite variants at the expense of others. When this biased structure is heated above the A_f temperature, it recovers back to its original shape. This process is called shape memory effect (SME), and there will be no net transformation strain with following forward transformation under zero applied stress. If the self-accommodated structure is permanently biased (generally by forming dislocations or internal stresses), large macroscopic strain will be experienced under zero applied stress with forward and back transformations. This process is called two-way shape memory effect (TWSME) [4,5].

It is well known that deformation of austenite in the range of A_f to a certain temperature (M_d) results in the stress induced martensitic transformation (SIM). Favored martensite variants are formed during loading and during unloading, but these martensite variants transform back to austenite since they are not chemically stable at that temperature. This deformation behavior is called pseudoelasticity (PE) or superelasticity. Pseudoelasticity is a more generic term than superelasticity. It also encompasses rubber-like behavior which is observed in some SMAs when the bars in the martensite phase are bent and aged to recover its original shape. Pseudoelasticity can be used for both martensite and austenite phases, whereas superelasticity is used for the parent phase only. As the temperature increases the stress required for inducing martensite also increases, exceeding the stress for dislocation slip which deteriorates the pseudoelastic response. Deformations at temperatures higher than M_d do not lead to SIM because dislocation slip is the only deformation mechanism. M_d is the highest temperature at which pseudoelasticity is observed.

Figure 1.1.4 shows the schematic of stress-strain response of a shape memory alloy. There are three possible deformation cases. Case I: If the material is initially in austenitic state, then in Stage I, elastic deformation of austenite occurs; in Stage II, stress

induced martensite forms; and in Stage III, slip deformation of martensite will occur. Case II: If the material is initially in the martensitic state, then in Stage I, elastic deformation of martensite occurs; Stage II, detwinning of martensite proceeds with some favored variants growing at the expense of others; and in Stage III, slip deformation of martensite will occur. Case III: If the initial material is a mixture of austenite and martensite phases, a mixture of the previous deformation types will take place. Upon unloading the martensitic structure will unload elastically in all cases which would be followed by pseudoelastic strain (back transformation from martensite to austenite) in Cases I and III. Further strain can be recovered if the deformed samples are heated above the A_f temperature. This process is known as shape memory effect (SME). The remaining permanent strain is inelastic strain as a result of dislocations formed during loading. The recoverable strain decreases with increased plastic deformation which mainly corresponds to the second plateau region in NiTi. This is because of the fact that slip formation inhibits reverse transformation due to the relaxation of stored elastic energy [6].

1.2 Brief history of SMAs

The first shape memory effect was discovered by a Swedish physicist, Arne Olender, in a AuCd alloy in 1932. The alloy was plastically deformed in a cold condition and it returned to its original shape after heating it. Later in 1938, the same effect was also observed in CuZn and CuAl [7]. In 1951, Chang and Read observed the shape memory effect in a AuCd alloy [8]. In 1961, Muldaver and Feder used an AuAgCd alloy in a thermally actuated electrical switch and took the first patent for a shape memory alloy [9]. But the turning point is the discovery of SME in equiatomic NiTi by Buehler and his co-workers at the U.S Naval Ordnance Laboratory (NOL) in 1962 [7]. An extensive study was launched to reveal the shape memory characteristics of NiTi, and the first application was Cryofit shrink-to-fit pipe couplers, which were used to join hydraulic lines of airplanes in 1970. In 1975 NiTi braces were used [9]. After the confirmation of biocompatibility of NiTi, the application field of NiTi has been tremendously enlarged. Emerging applications of NiTi shape memory alloys include micro-electro-mechanical systems (MEMS), biomedical devices and implants such as

stents for opening up arteries ($\sim 10^5$ cycles per day), and deployable aerospace applications like actuators for maneuvering the wings of an aircraft. Application of shape memory alloys are summarized well by others and will not be discussed here [1,7,10,11].

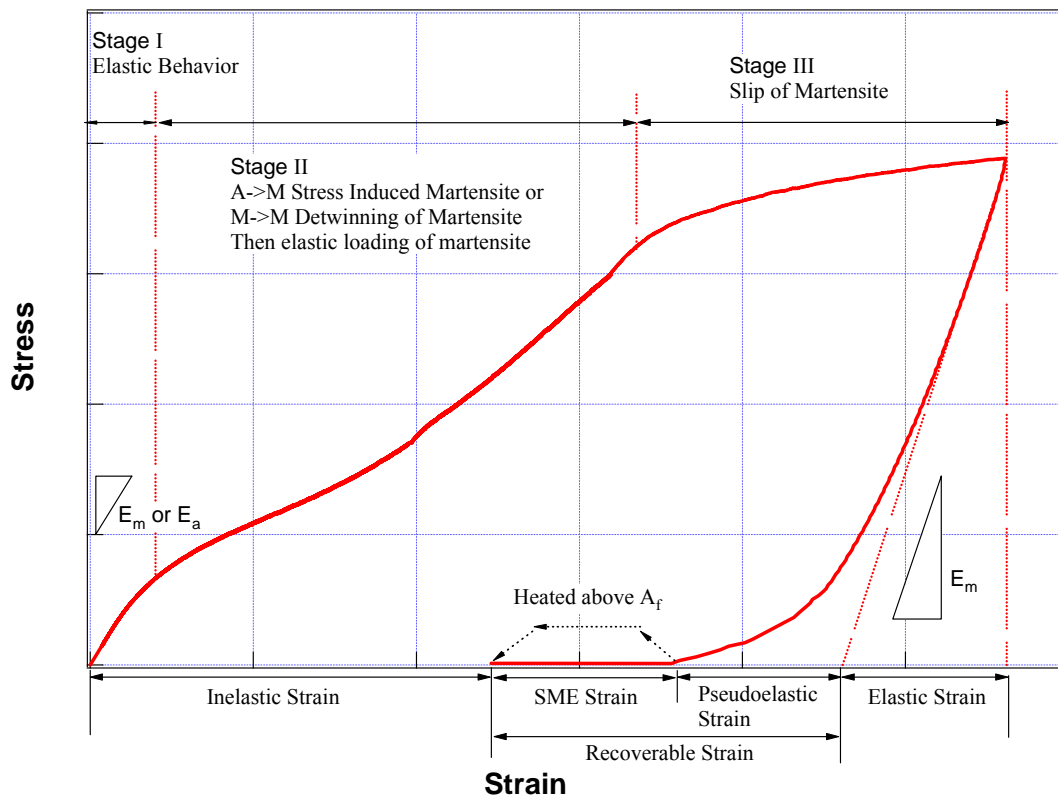


Figure 1.1.4 A schematic of stress-strain behavior of shape memory alloys.

1.3 Phase diagrams

Figure 1.3.1 shows the phase diagram of NiTi. The central part of the Figure 1.3.1 where NiTi transforms to B19' martensitic phase is important. On the nickel rich side Ti_3Ni_4 , Ti_2Ni_3 and $TiNi_3$ precipitation formation has been reported and resulted in confusion for a while, whether there is a eutectoid reaction or not. But it is understood that the Ti_3Ni_4 and Ti_2Ni_3 phases are intermediate phases and they transform to equilibrium $TiNi_3$ phase with longer aging time [12]. For the Ti rich side the equilibrium phase is Ti_2Ni but Ti is so active that it easily combines with oxygen and carbon at high temperatures. The order-disorder transition temperature is at 1090°C as indicated by dotted line on the phase diagram [13].

As it can be deduced from the phase diagram, the composition range for the ordered B2 phase NiTi is from 49 to 57 at% Ni at 1090°C. The composition range should be kept close to equiatomic composition since precipitations do not demonstrate shape memory behavior. The phase diagram of NiTi has been used to improve the shape memory characteristics by formation of precipitates. As will be discussed later, precipitates change the transformation temperatures (TTs), strength and PE substantially.

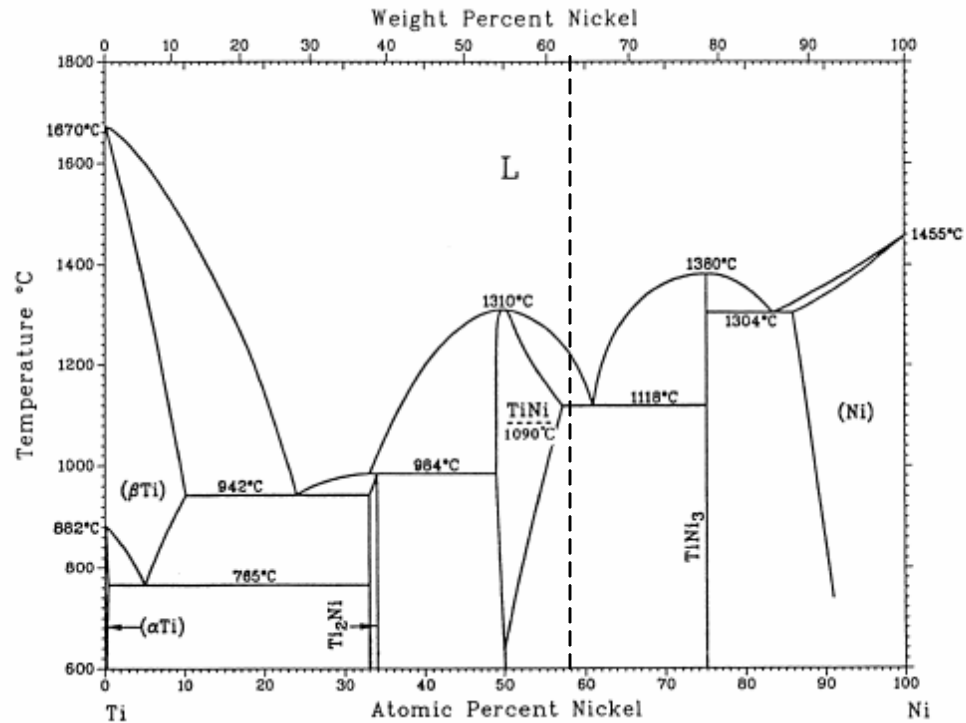


Figure 1.3.1 Phase diagram of NiTi [13].

1.4 Crystal structures

It is very important to know the crystal structure of phases in order to understand their physical properties. The parent phase of NiTi has BCC B2 crystal structure which is ordered like CsCl type with lattice constants of about $a=0.301\text{nm}$ [1].

So far three martensitic phases are determined for NiTi and NiTiX alloy systems. B19' is most common phase observed in NiTi and its alloys. Its space group is $P2_1/m$ and has a monoclinic crystal structure with lattice parameters of $a=0.2898\text{ nm}$, $b=0.4108\text{ nm}$ and $c=0.4646\text{ nm}$ and $\beta=97.78^\circ$ for Ti-49.2 at% Ni [14]. The lattice parameters are composition dependent. The other phase, the so called “premartensitic phase” is rhombohedral R-phase which belongs to the space group of $P3$ with lattice parameters of

about $a_R = 0.732\text{nm}$ and $c_R = 0.532\text{nm}$ [15]. The R-phase is elongated 0.94% along the parent $[111]_{B2}$ orientation. This is one order smaller than that for the B19' martensite [2]. B19 is an orthorhombic phase with lattice constants of $a_o = 0.29\text{nm}$, $b_o = 0.425\text{nm}$, and $c_o = 0.45\text{nm}$ [16]. Structural relationships of the parent phase and two martensitic phases are shown in Figure 1.4.1 [17].

Aging, cold working and annealing, thermal cycling, increasing Ni content and alloying of NiTi (eg. NiTiFe and NiTiAl) could promote R-phase transformation by suppressing the M_s temperature [2,18]. B2 to R-phase transformation results in very small shape change ($\sim 0.8\%$) but also has very small temperature hysteresis. B19 is observed in ternary alloys of NiTi. For NiTiCu alloys, the transformation behavior changes from one stage B2-B19' to B2-B19-B19' and to B2-B19 with increasing Cu content [16,19]. The amount of transformation strain of B19 is between the R and B19' phases. Stability of mechanical and thermal properties under thermomechanical treatments, lower hysteresis due to small transformation strain and lower cost due to Cu addition make NiTiCu suitable for industrial applications.

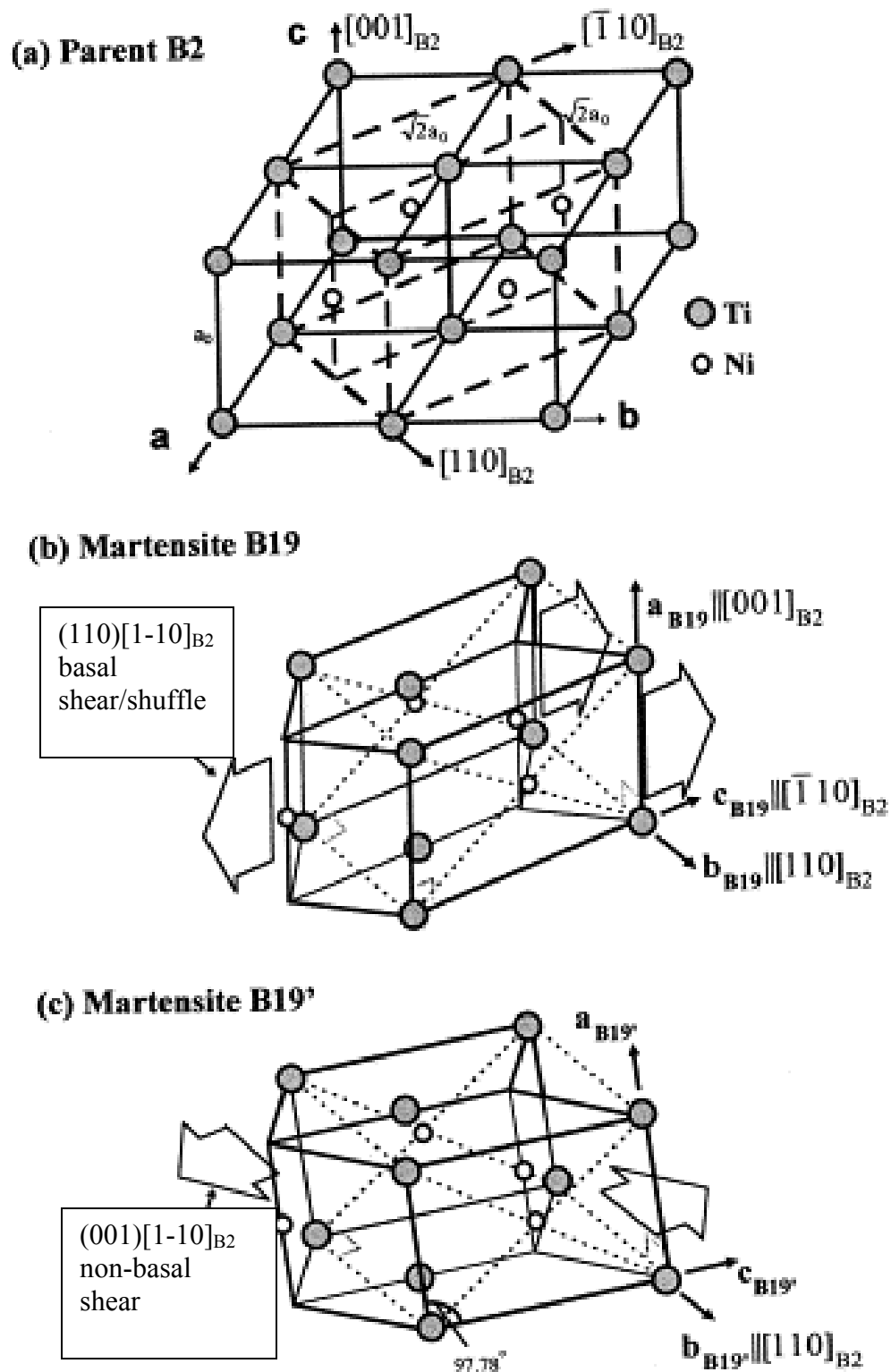


Figure 1.4.1 Structural relationship among cubic parent phase (B2) and two kinds of martensites B19 and B19', (a) the parent phase B2, (b) orthorhombic martensite B19, (c) monoclinic B19' martensite of NiTi [17].

1.5 Self accommodation

As explained previously, in order to minimize the overall strain energy, martensite variants form self-accommodated structures. For NiTi each martensitic phase has a different self accommodating morphology as described subsequently.

There are 12 lattice correspondences between the parent B2 and martensite B19' phase resulting in 24 martensite variants. They form a triangular self accommodating morphology as shown in Figure 1.5.1. The interphase between each two of three variants is a twin plane. There are 16 groupings which form a triangular self accommodating morphology around each of the $[001]_{B2}$ poles, resulting in 48 possible combinations of variants for such triangles [18]. In single crystal NiTi there are 24 different martensite correspondence variant pairs (CVPs). A CVP is a formal term for a martensite plate since it contains two twin-related martensite single-crystal variants. In the detwinning process, the CVP is transformed from two twin related martensite single crystals into a single crystal of martensite resulting in additional transformation strain. Thus detwinning is the growth of one martensite variant (chosen by stress state and orientation) at the expense of others.

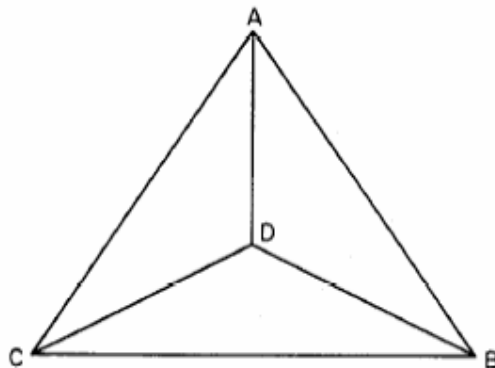


Figure 1.5.1 Self accommodating morphology of B19' [20].

There are 4 equivalent lattice correspondences between the B2 and R phases. Figure 1.5.2 shows a typical example of a self-accommodating structure. There are two types of morphology, one is a straight band morphology that corresponds to the view from $[100]_{B2}$ and $[010]_{B2}$ and the other one is a herring-bone (saw-tooth) morphology that corresponds to the view from $[001]_{B2}$ of Figure 1.5.2 [2].

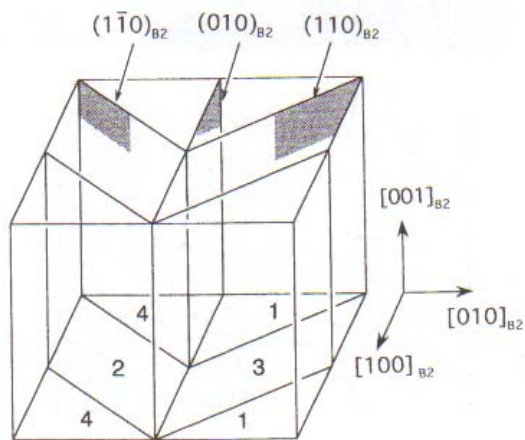


Figure 1.5.2 Self accommodating morphology of R phase [2].

For orthorhombic B19 phase there are 6 equivalent lattice correspondences between the parent and martensitic phases. Again a triangular morphology is observed in the $[111]_{B2}$ orientation as shown in Figure 1.5.3 [2].

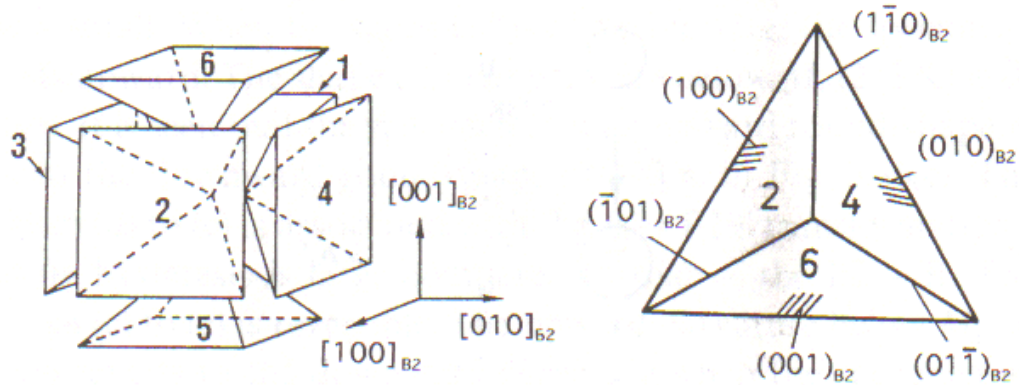


Figure 1.5.3 Self accommodating morphology of B19 phase [2].

In all self-accommodating structures, martensite variants have twin relations with each other and when an external force is applied the most favorable variant grows at the expense of others, resulting in a net shape change.

1.6 Ductility of NiTi

Although most of the intermetallics are brittle, NiTi has a very peculiar ductile nature. The main reasons for this ductility are the low anisotropy factor, small grain size, low strength for slip near M_s , and availability of twinning modes in the martensitic phase. The anisotropy factor of NiTi is ~ 2 and grain size is $\sim 30\mu\text{m}$ where for the other intermetallic alloys they are around 15 and $\sim 1-5\text{ mm}$, respectively. A high anisotropy factor results in grain boundary fracture in most intermetallics. Also the low elastic constant c_{44} leads to low stress for the activation of the $\{110\}\langle 001\rangle$ slip system in NiTi which enhances ductility.

1.7 Determination of transformation temperatures

Resistivity is the oldest method to characterize transformation temperatures (TTs), but it is difficult to distinguish the peaks and determine the TTs for untrained researcher. Also this method is very sensitive to thermal cycling that changes the resistivity curves.

Constraint cycling is another method that can be used to determine the TTs by applying a very small stress and then thermally cycling under this stress and recording the strain response. This method would result in slightly shifted TTs as a result of applied stress, but this method is very useful to characterize TTs under different stress levels and find the Clausius-Clapeyron relationship.

Differential Scanning Calorimetry (DSC) is the most common method to determine the TTs. Because of the fact that forward transformation is exothermic and reverse transformation is endothermic, the TTs can be determined by the change in heat loss curve during cooling and heating. A schematic of a DSC curve and determination of TTs by the intersecting slopes method is shown in Figure 1.7.1. Advantages of DSC are: ease of determining TTs, small sample size (10mg) needed, ease to operate and fast response.

Magnetic susceptibility or magnetization curves under a constant applied magnetic field lower than saturation values are also very effective to determine the TTs, especially if at least one of the phases is ferromagnetic, then a strong magnetization response can be obtained under a constant applied magnetic field, and its change with temperature can be used to determine the TTs.

Acoustic emission and in-situ observation techniques are other methods to determine the TTs. The former technique determines the acoustic bursts that occur during interphase movement where the latter uses optical or electron microscopy techniques to observe the changes on the surface of specimens during thermal cycling.

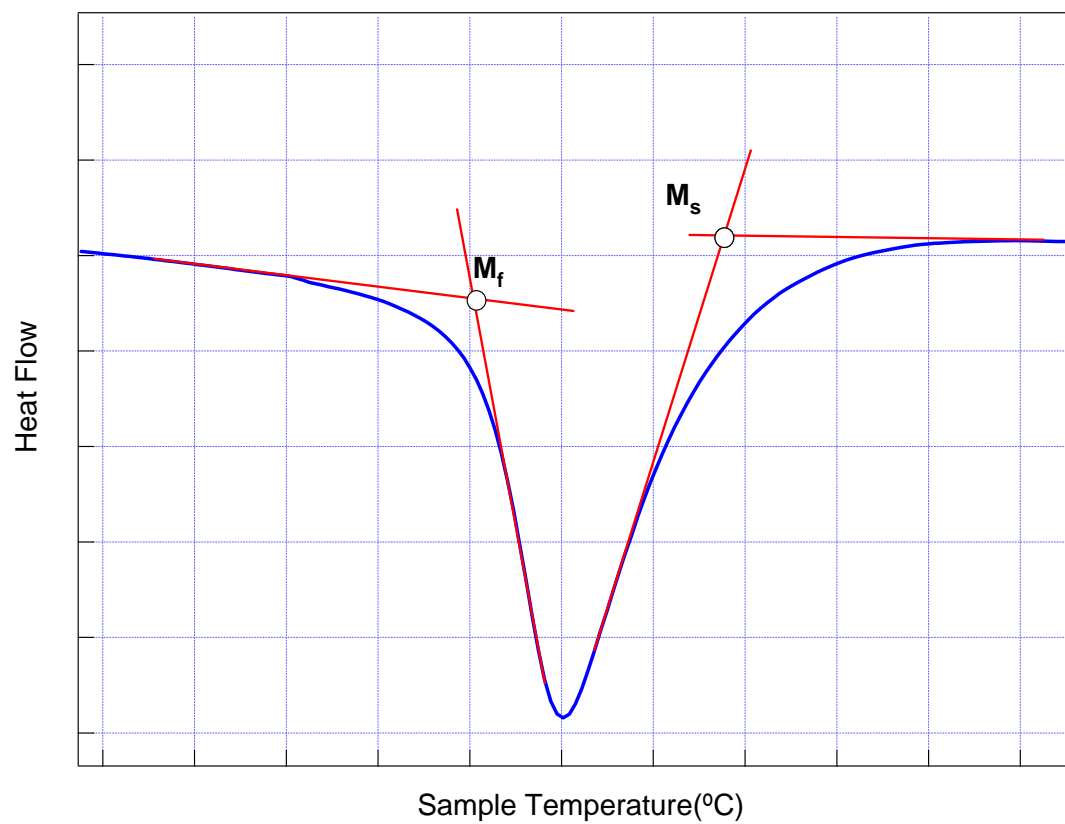


Figure 1.7.1 Schematic of intersecting slope method for finding transformation temperatures from DSC response.

CHAPTER II

MOTIVATION

Use of shape memory alloys is limited if a high number of thermal or mechanical cycles are applied, because martensitic transformation is sometimes accompanied by dislocation formation in addition to internal twinning. This leads to creep and poor fatigue response.

In most applications, these alloys are subjected to a high number of repeated cycles either by thermal activation or by the application of cyclic load. Table 2.1 summarizes some typical SMA applications, underlying SM effects and expected fatigue lives N_f [21].

Table 2.1 Some typical SMA applications, underlying SM effects and expected fatigue lives N_f [21].

Application	SM effect	Expected fatigue lives N_f
Thermal valve	Oneway SME	10^4 Cycles
Positioning	TWSME	10^5 Cycles
Robot gripper	TWSME	10^6 Cycles
Orthodontic wire	PE	10^5 Cycles
Stents	PE	10^8 Cycles
Damping, internal friction	PE	10^8 Cycles

Thus cyclic degradation of NiTi alloys presents a critical roadblock for the use of these active materials for applications that require a high number of cycles. Change in TTs, reduction in the transformation strain, and an increase in irrecoverable (creep) strain could be the consequences of cyclic degradation. Thus improving the cyclic stability and fatigue resistance of shape memory alloys is of utmost importance.

Probable reasons for unstable mechanical and thermal response are introduction of primary defects like dislocations during the austenite to martensite transformation and

poor strength of the parent phase [22-28]. In their work on microstructural evolution during the mechanical cycling of NiTi single crystals, Hurley *et al.* [25] performed experiments in tension and compression along two different orientations ([100] and [111]). With intermittent transmission electron microscopy (TEM) observations, they concluded that maximum cyclic degradation occurs in the first 20 cycles of loading and that the motion of the martensite/parent interface produces defects.

Possible solutions to minimize and/or avoid the formation of lattice dislocations during cycling is to increase the strength of the parent phase [22,23,24,26]. Thermomechanical treatment (TMT) using Equal Channel Angular Extrusion (ECAE) provides a way to achieve this goal. Possible results of TMT can include grain refinement, an increase in dislocation density (strain hardening) via ausforming or marforming, crystallographic texture strengthening and precipitation hardening [22,23,24,26]. TMT is a combination of plastic deformation and subsequent annealing heat treatment. Annealing heat treatment may or may not be necessary depending on the temperature at which the deformation is carried out or the way deformation is carried out (i.e. stress state and strain level). Usually, deformation above the austenite finish (A_f) suppresses the transformation to a very low transformation temperatures whereas low temperature annealing heat treatment leads to recovery. A low temperature annealing treatment is also necessary to preserve the ductility of the alloys [29-35].

Aging NiTi at low temperatures (>350 °C) in compositions greater than 50.5 at % Ni leads to nucleation of precipitates which strengthen the alloy by pinning the dislocations. Precipitates also act as preferential sites for the nucleation of martensite crystals due to the stress field around them [36].

Various severe plastic deformation techniques (SPD) like High Pressure Torsion (HPT) and Equal Channel Angular Extrusion (ECAE) have been utilized recently on shape memory alloys by Valiev *et al.* [33-35] and also in our previous study on marforming of NiTi [37].

Valiev *et al.* [33,34] demonstrated in their study on equiatomic and nickel rich NiTi alloys that SPD using high pressure torsion (HPT) leads to amorphization and nanograin formation after subsequent annealing. They studied the effects of thermomechanical treatment on microstructure and conventional mechanical properties

(strength levels and ductility) of the alloy, but they did not report any result on the effect of heavily deformed microstructures on shape memory properties like transformation behavior, formation of the R-phase, pseudoelasticity or recoverable strain. Moreover, the sample size (10-12 mm in diameter and 0.3-0.5 mm thickness) that can be obtained by HPT is relatively small for performing an extensive investigation on shape memory and pseudoelasticity properties and the strain is not usually uniform throughout the sample.

In many previous studies involving microstructural evolution in NiTi during thermomechanical treatments and its effects on cyclic stability, less than 100 pseudoelasticity cycles have been applied and no correlation between thermal hysteresis and cyclic stability were drawn [22-26]. Hosogi et al. [24] and Mertmann *et al.* [30] on the other hand completed up to 1000 cycles of loading and unloading on cold worked samples but failed to recover 100% strain after the 1000 cycles.

In this study ECAE is used as a tool for SPD with as many as 1000 pseudoelasticity cycles performed on ECAE processed samples, and a comparison is made with conventional cold drawn, precipitation hardened and solutionized material before and after selective heat treatments. ECAE permits the application of a large amount of uniform strain without a reduction in work piece cross section and results in large processed billets. ECAE is superior to the other techniques because of the formation of uniform microstructures, control over the development of grain morphology, formation of specific texture and ease of process [38]. Figure 2.1 is a schematic representation of the ECAE process. Load is applied from the top of the vertical channel, and the billet is deformed in the shear zone and extruded from the horizontal channel. The angle between the two channels is 90° in the present case. The passage of a billet through such a tool produces simple shear in the bar at the channel intersection plane. SPD of NiTi using ECAE is challenging, as NiTi has high flow strength in austenite and its ductility is limited. For a successful extrusion, ECAE tool design should be able handle high strength levels by limiting friction possibly through a sliding walls concept [39].

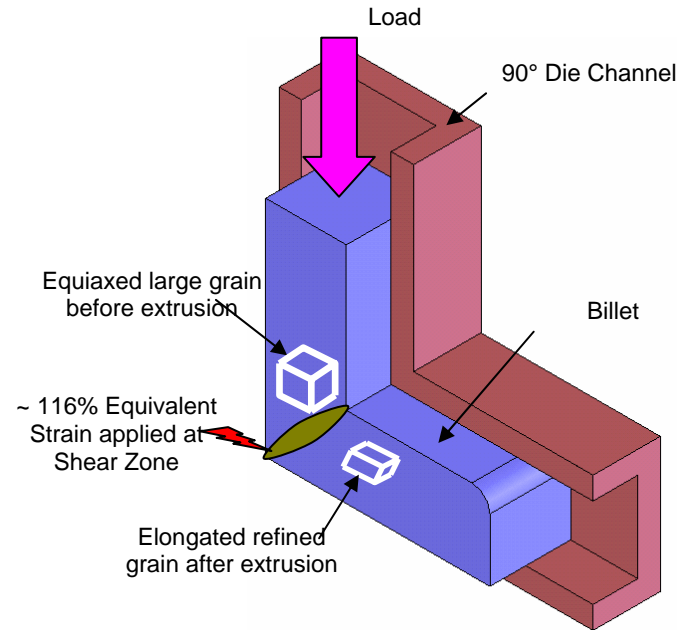


Figure 2.1 Schematic representation of ECAE process

In the present study, effects of SPD using ECAE are investigated on the microstructure, transformation behavior and thermomechanical cyclic stability for a nickel rich NiTi alloy (50.7 and 50.8 at % Ni). We discuss the effects of SPD on mechanical twinning formation in austenite and propose a mechanism which involves forward and reverse martensitic transformation. The objective is to establish a processing-microstructure-property relationship. Observed unique microstructural features in ECAE processed material show that ausforming with ECAE is a powerful tool for improving the cyclic response of Ni rich NiTi alloys and opens new opportunities for grain boundary engineering in SMAs. ECAE processed samples shows promising results and an outstanding improvement in the cyclic stability by recovering 100% strain up to the 1000th cycle as compared to less than 50% recoverable strain in conventional cold drawn and solutionized material.

CHAPTER III

EXPERIMENTAL PROCEDURE

50.8 at % Ni-Ti alloy samples were received from Special Metals Corp., New Hartford, New York in the cold drawn condition. The cold drawn material was solution heat treated at 1000 °C for one hour and water quenched before ECAE. The martensite start (M_s), austenite start (A_s) and austenite finish (A_f) temperatures were found to be -30 °C, -30 °C and 4 °C, respectively, in the solutionized form.

3.1 Extrusions

For ECAE at room temperature (RT) an 8 mm diameter NiTi billet was canned in Ni, and for 450 °C extrusion a 10 mm diameter billet was canned in stainless steel. The can size was 25.4 mm square by 127 mm length, and it was used to minimize tool wear during extrusions. The ECAE was conducted at RT (just above A_f , ECAE at RT), and at 450°C (well above A_f , ECAE at 450 °C) with a die angle of 90° (equivalent strain ~ 1.16 at each pass). For the ECAE at 450 °C, the billet was kept at 450 °C for one hr in a furnace prior to extrusion, transferred to the ECAE tool which was held at 300 °C as quickly as possible (in less than 5 seconds) and extruded at a rate of 5 mm/sec. The RT extrusion was conducted at a rate of 0.025 mm/sec to minimize the deformation heating. The reason for the fast extrusion at 450 °C is that the available ECAE tool can only be heated up to 300 °C, and fast extrusions are necessary for extrusions above this temperature (300 °C) to eliminate the die chilling effect. Thus, the 450 °C extrusions were nonisothermal. Only one pass was applied because the load levels were very high, and a second pass could cause catastrophic failure to the tool. The solutionized material was aged at 450 °C for one hr for comparison with the ECAE at 450 °C sample properties. The ECAE at RT sample was annealed at 450 °C to investigate the annealing microstructures. Table 3.1.1 summarizes the extrusion conditions including extrusion route, initial condition of billets, can type and extrusion rate. Figure 3.1.1 shows the 250 ton extrusion press at Texas A&M University.

Table 3.1.1 Summary of extrusions

Extrusion	Material	Extr. Route	Initial condition of the Billets			Time	Matl	Can Type Dimensions (mm)	Extr. Rate mm/sec
			Dimensions (mm)	Condition	Temperature				
ECAE at RT	50.8 at % NiTi	1A	8 mm dia. x 76 mm length	Solutionized	1000°C	1h	Ni	25.4 mm square x 127 mm length	0.025
ECAE at 450°C	50.8 at % NiTi	1A	10 mm dia. x 76 mm length	Aged	450°C	1h	SS	25.4 mm square x 127 mm length	5

**Figure 3.1.1** 250 ton extrusion press at Texas A&M University

3.2 Calorimetric analysis

A Perkin-Elmer Pyris-I differential scanning calorimeter (DSC) was used to explore the effects of ECAE on resulting transformation temperatures, R-phase formation, and the effect of short annealing heat treatment. 20-30 mg samples were used for the calorimetric analysis.

3.3 Microstructural evolution

The microstructure of the materials was investigated using transmission electron microscopy (TEM). TEM foils perpendicular to the extrusion direction were prepared from the samples by mechanical thinning down to 100 μm , followed by twin-jet electro polishing with a solution of 20 volume % H_2SO_4 in a methanol solution at 25 $^\circ\text{C}$. A JEOL 2010 microscope operated at a nominal accelerating voltage of 200 kV was utilized. The main idea was to investigate the microstructural evolution after ECAE and some selected heat treatments.

3.4 Thermomechanical testing

The thermomechanical cycles and mechanical experiments were conducted using square, 4 mm wide by 8 mm long compression specimens. Compression specimens were electron discharge machine (EDM) wire cut from as-received, as-received + annealed at 450 $^\circ\text{C}$ for one hr, solutionized, solutionized + aged at 450 $^\circ\text{C}$ for one hr and ECAE processed samples. Three types of experiments were performed in compression:

1. Pseudoelastic cycling by incrementally increasing the strain up to approximately 8% at $A_f + 20$ $^\circ\text{C}$. The main goal of these experiments was to find out the yield stress for martensite (start of second plateau), the stress for inducing martensite (SIM), pseudoelastic recoverable strain, and the maximum strain level at which the transformation is purely a SIM without moving into the elastic region of martensite.
2. Thermal cycling between a temperature below M_f (martensite finish) and a temperature above A_f (austenite finish) at various stress levels while recording the strain values. The main goal of these experiments was to investigate the stress

- dependence of thermal hysteresis, determine the transformation strain, irrecoverable strain and construct a Clausius-Clapeyron curve.
3. Pseudoelastic cycling to 3% strain at $A_f + 20^\circ\text{C}$ for up to 1000 cycles. The main goal of these experiments is to observe the effect of mechanical cycling on recoverable strain and stress hysteresis for different deformation and heat treatment conditions.

The load was measured with a load cell and strain was measured with a miniature Materials Test Systems (MTS) extensometer with a 3 mm gage length. The use of the miniature extensometer circumvents the end effects associated with crosshead displacement measurements. Heating the samples was achieved by conduction through the compression plates which were heated by heating bands. The temperature was measured using a type K thermocouple. Figure 3.4.1 shows the servohydraulic MTS test frame used for thermomechanical testing and Figure 3.4.2 shows the miniature Materials Test Systems (MTS) extensometer with a 3 mm gage length.

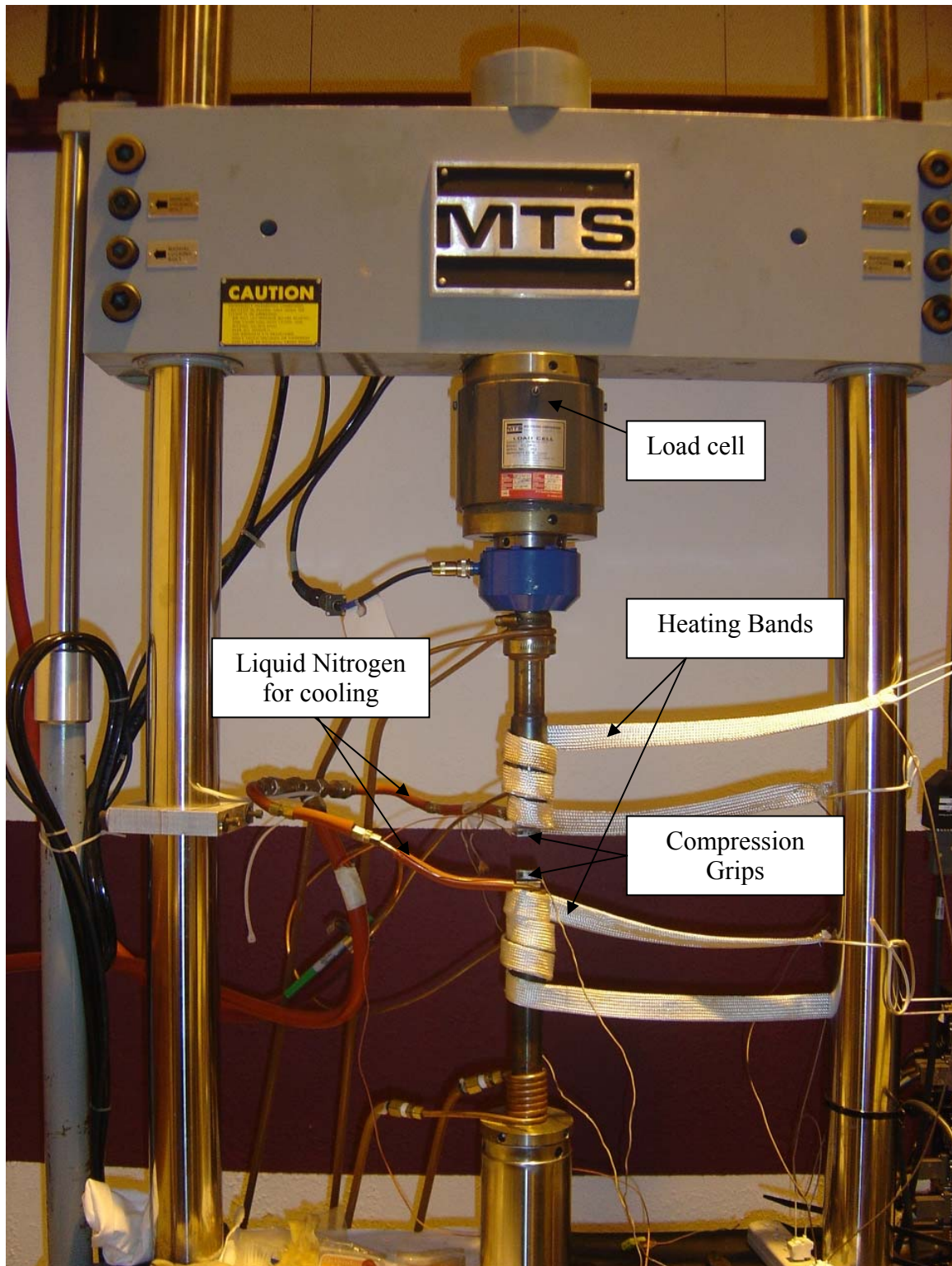


Figure 3.4.1 Servohydraulic MTS test frame used for thermomechanical testing.

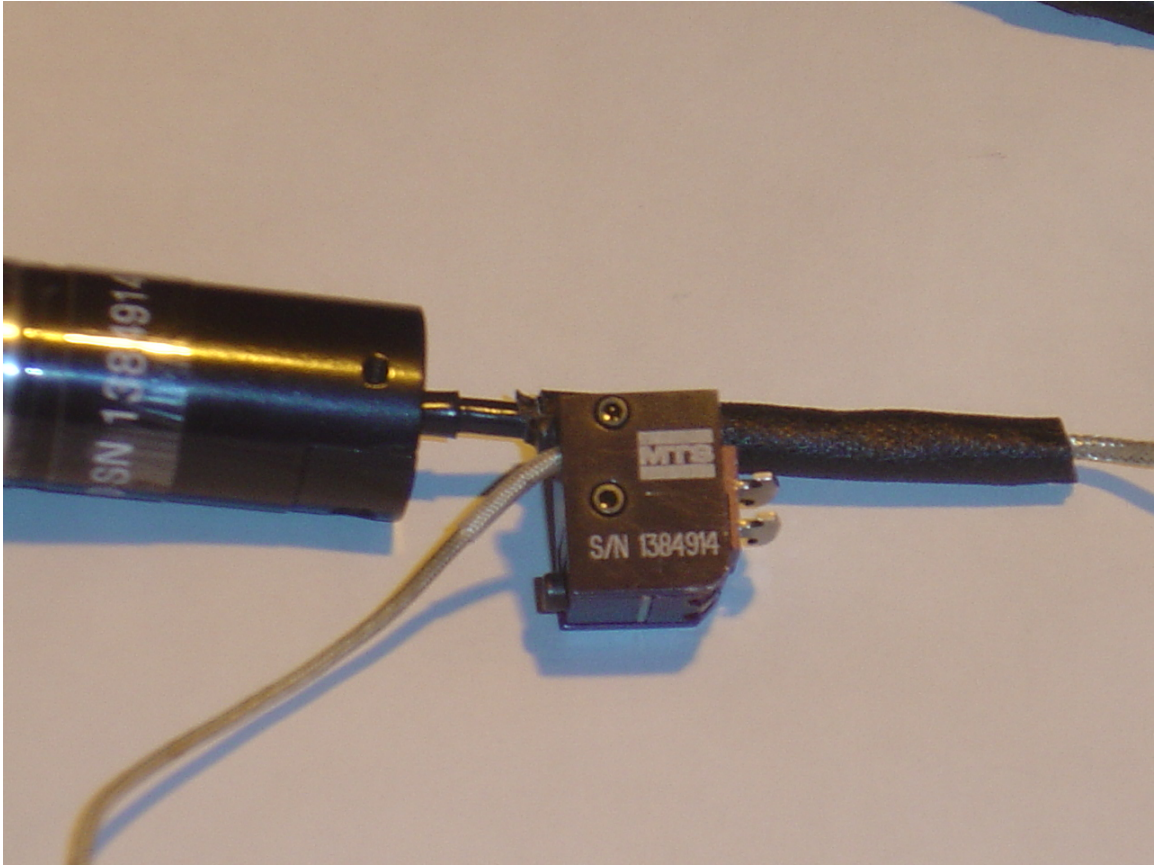


Figure 3.4.2 Miniature Materials Test Systems (MTS) extensometer with a 3 mm gage length.

CHAPTER IV

RESULTS AND DISCUSSION

4.1 Calorimetric analysis

The main goal of calorimetric analysis is to investigate the effects of SPD via ECAE on TTs, transformation behavior and formation of R-phase. ECAE processed samples were annealed in the DSC for 1 min at various temperatures ranging from 100 °C to 600 °C at an interval of 50 °C. The effects of recovery and recrystallization process on transformation behaviour were investigated. Figure 4.1.1 shows the DSC response of as-received, solutionized, and ECAE processed materials. No transformation was detected in the sample ECAE processed at RT when thermally cycled in the DSC from -60 °C to 100 °C. Therefore, a 450 °C 30 min low temperature annealing treatment was done, and then DSC was performed on this material. It is interesting to see single stage R-phase to austenite transformation during heating and austenite to R-phase transformation during cooling in the ECAE at RT sample after annealing treatment. The R-phase is a rhombohedral phase which is usually observed upon cooling from the parent phase before the formation of B19' monoclinic martensite under certain conditions such as cold working, thermal cycling, aging and third element alloying [40]. But in this case no martensitic transformation was observed at temperatures as low as -60 °C which is the lower working limit of the DSC used, indicating that the M_s and M_f temperatures are suppressed below -60°C. In Figure 4.1.1, all the other transformations (except ECAE at RT, annealed at 450°C for 30min) are one stage (i.e. from austenite to martensite on cooling and from martensite to austenite on heating) without the formation of an R-phase. There is a considerable increase in the M_s temperature for solutionized material as compared to as-received material which is attributed to complete annihilation of dislocations, recovery, recrystallization and grain growth. The A_s and A_f temperatures for the material ECAE processed at 450°C are comparable to as-received and solutionized materials, but there is a considerable drop (-35°C as compared to solutionized material) in the M_s temperature and the temperature range at which the transformation occurs is narrower.

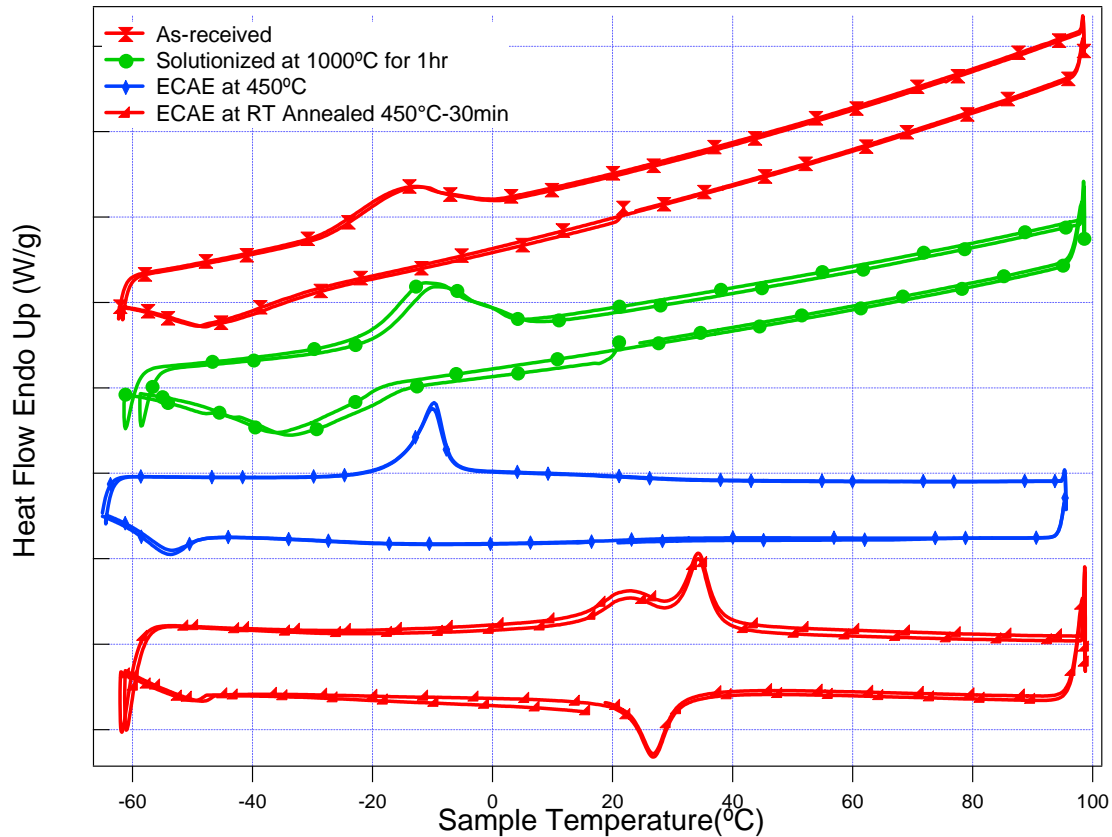


Figure 4.1.1 DSC response of as-received, solutionized and ECAE processed material.

A low temperature heat treatment at 450°C for one hr was performed on as-received and solutionized material to form Ni rich Ni_4Ti_3 precipitates [36]. DSC was performed on these samples, and an interesting 3 stage transformation was observed in solutionized material after aging. Figure 4.1.2 shows the DSC response of solutionized material after the specified aging heat treatment. A possible explanation for the observed three stage transformation in aged material is a considerable precipitation reaction which usually starts to occur at 400 °C and above in 50.8 at % Ni-Ti alloy [41]. These precipitates trigger early nucleation of martensite crystals in their vicinity due to the stress fields around them. And later matrix starts to transform thus giving three peaks: one from austenite to R-phase, a second from R-phase to martensite near precipitates and a third from R-phase to martensite for the entire matrix.

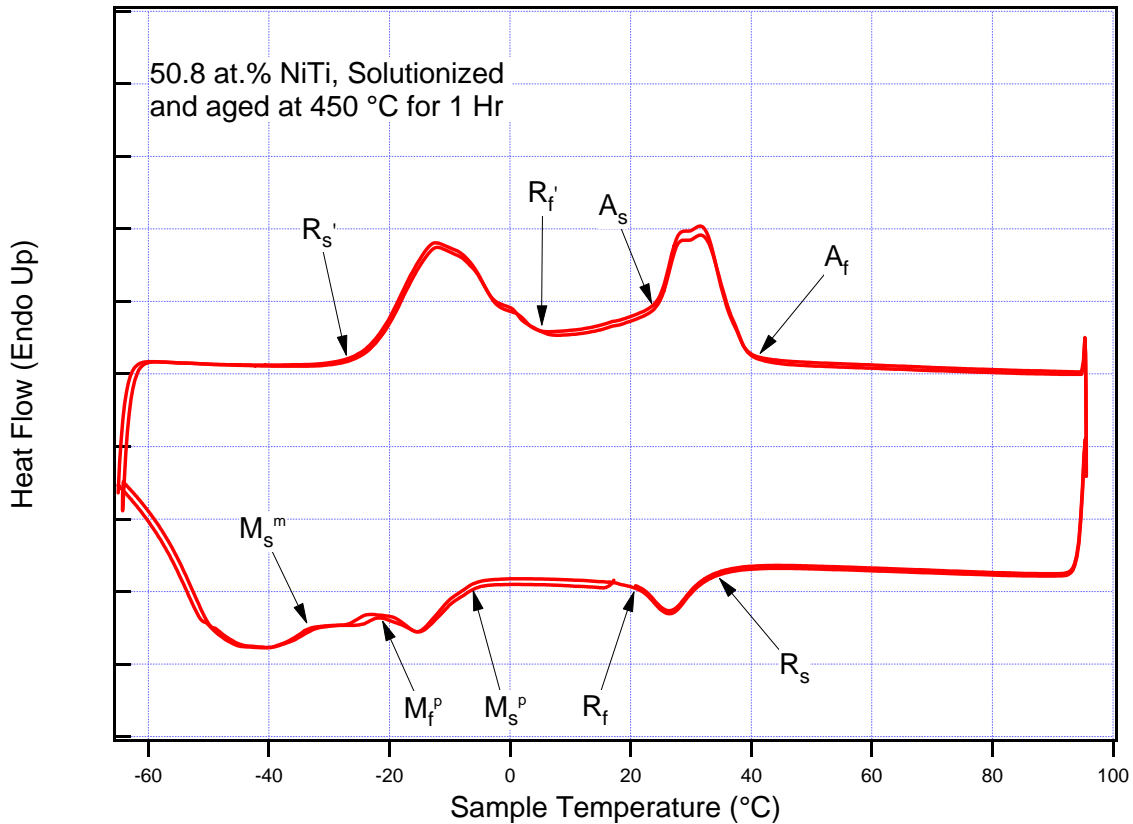


Figure 4.1.2 DSC response of the material solutionized and aged at 450 °C for 1 hour showing a three stage martensitic transformation, i.e. austenite to R-phase transformation, R-phase to martensite transformation near precipitates (M^p), and R-phase to martensite transformation away from precipitates (M^m).

The ECAE deformed materials were annealed at various temperatures ranging from 100°C to 600°C at an interval of 50 °C to observe the effect of annealing temperatures on transformation behavior of ECAE processed material. Figures 4.1.3 (a) and (b) show the DSC response of ECAE at RT and ECAE at 450 °C, respectively, whereas Figures 4.1.3 (c) and (d) are plots of TTs as a function of annealing temperature for ECAE at RT and ECAE at 450 °C samples, respectively. TTs of the solutionized and

solutionized + aged samples are also included in Figures 4.1.3 (c) and (d), respectively, to show the initial conditions of the samples before ECAE.

As can be seen from the Figure 4.1.3 (a) and (b), the transformation occasionally proceeds in two stages with the formation of R-phase. For the case of ECAE at RT, a transformation was observed only after annealing at 200°C for 30min; however, it was an Austenite (B2) to R and R to B2 transformation without the formation of B19' down to -60 °C. M_s and M_f are above -60 °C only after annealing at 500 °C and increase with increasing annealing temperature (Figure 4.1.3 (c)). The temperature range of martensite to austenite and austenite to R-phase transformation decreases with increasing annealing temperature (Figure 4.1.3 (c)) due to annihilation of dislocations and a decrease in the resistance to the phase boundary motion. For ECAE at 450°C, almost all the reverse TTs (i.e. A_s and A_f) are constant up to 300°C after which they increase till 400°C and then remain constant (Figure 4.1.3 (d)). This increase is probably because of the formation of Ni-rich precipitates and Ni depletion in the matrix. R-phase transformation was seen above 300°C, while the M_s is constant up to 400 °C after which it increases continuously (Figure 4.1.3 (d)). Four stage transformation cycles are evident for ECAE @ RT samples after annealing at 450 and 500 °C (Figure 4.1.3 (a)) and for ECAE @ 450 °C samples after annealing at 400 and 450 °C (Figure 4.1.3 (b)). For the former, the reason for multi-stage transformation is heavy deformation and partial recovery. For later, it is probably precipitation. It will be shown subsequently that annealing ECAE at RT material at 450 °C did not yield any precipitates.

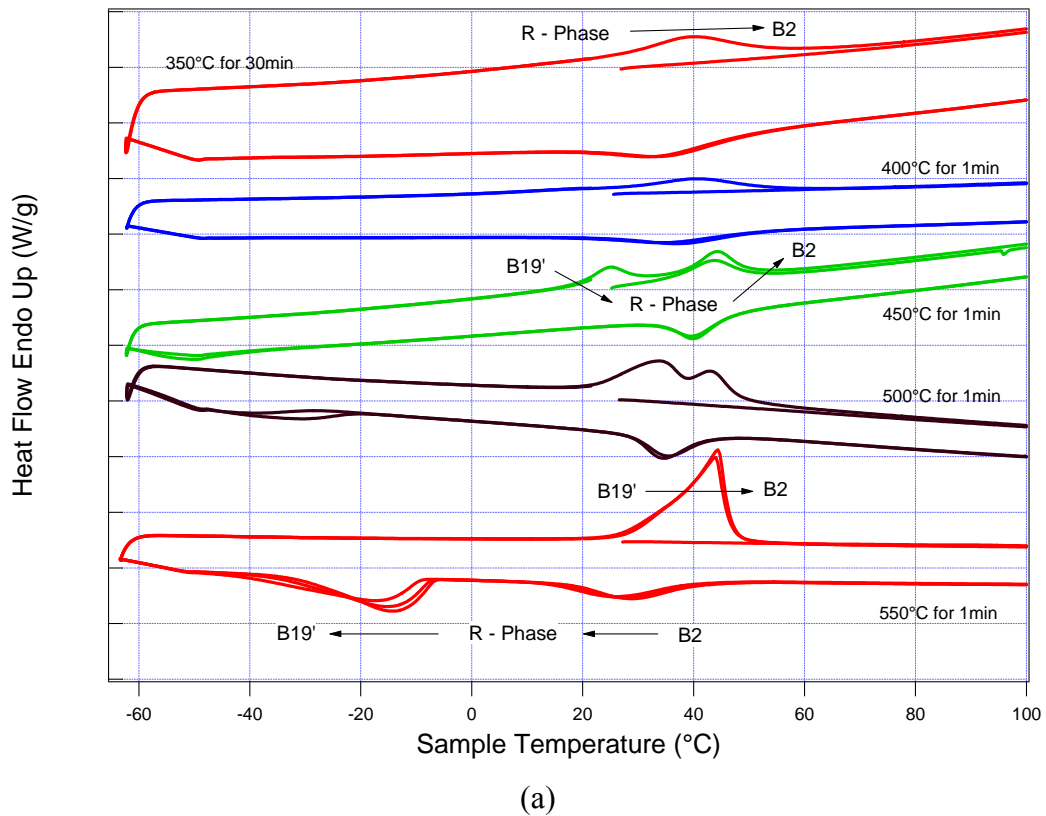
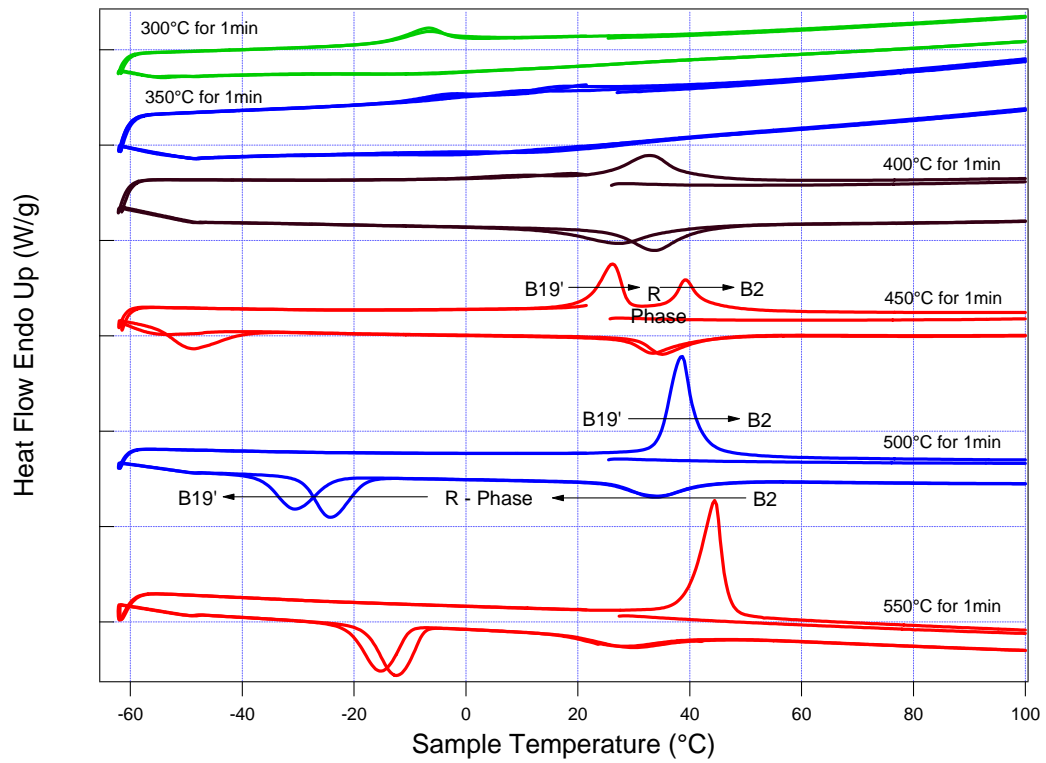
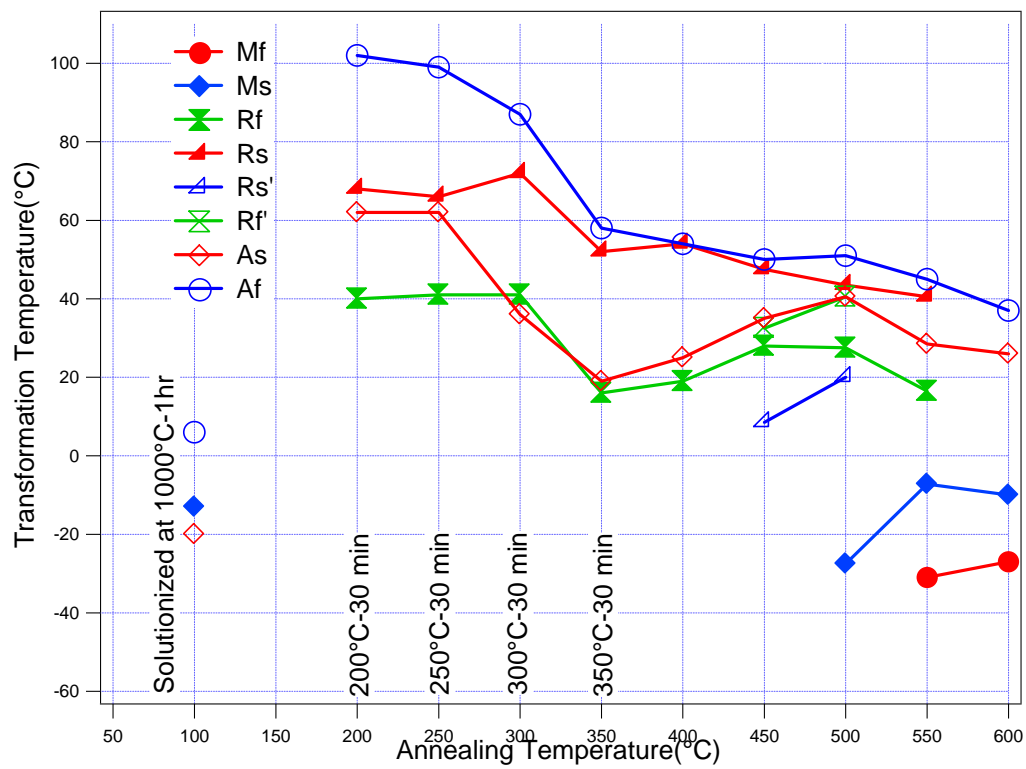


Figure 4.1.3 Effect of annealing temperature on the transformation behavior of ECAE processed material (a) DSC response of ECAE at RT, (b) DSC response of ECAE at 450 °C, (c) TTs for ECAE at RT, and (d) TTs for ECAE at 450 °C samples. TTs of the solutionized and solutionized + aged samples are also included in Figures (c) and (d), respectively, to show the initial conditions of the samples before ECAE.

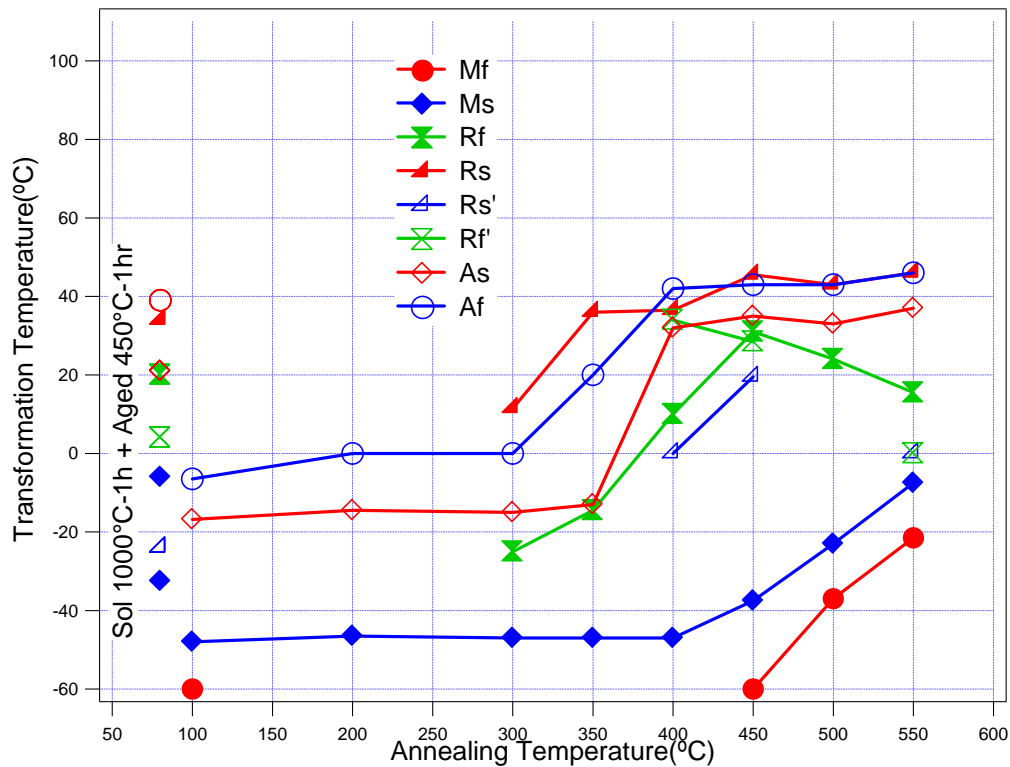


(b)



(c)

Figure 4.1.3 Continued.



(d)

Figure 4.1.3 Continued.

In consideration of the observed differences in TTs, three factors should be considered: 1) How does annealing modify the high dislocation density structure in ECAE samples and what is the effect of new microstructure on TTs?; 2) How does precipitation change the TTs?; and 3) How would the heavily deformed structure affect precipitation? The low temperature annealing of a heavily deformed structure would cause partial recovery and increase in TT because of decreased dislocation density. Secondly, the considerable precipitation reaction usually starts to occur at 400 °C and above in 50.8 at % Ni-Ti alloy [41]. The precipitation has three major effects on TTs. TTs increase due to the formation of Ni-rich precipitates and Ni depletion in the matrix. Secondly, the stress field of coherent precipitates can cause an increase in TTs. Moreover, coherent precipitates trigger R-phase transformation. Thirdly, if the volume fraction of coherent precipitates is low, three stage transformation may occur upon

cooling (i.e. A \rightarrow R transformation, R \rightarrow M transformation near precipitates, and R \rightarrow M transformation away from precipitates) as shown in Figure 4.1.2 for the case of 50.8 at.% Ni-Ti after aging solutionized material at 450 °C for 1 hour. The third factor that needs to be considered is the effect of heavily deformed structures on precipitate formation. Dislocations are favorable nucleation sites for precipitates [42], and short-circuit diffusion paths for solutes [43, 44]. This results in faster and coarser precipitation on dislocations. Therefore, precipitation would accelerate and start at lower temperatures in heavily deformed structures. Thus, annealing of ECAE samples is expected to cause faster precipitate reactions and coarser precipitates; however, this was not observed as discussed subsequently. This unexpected behavior is probably due to the fact that the interaction between dislocations and solutes may result in a solute flux to dislocations [45, 46, 47]. Therefore a lower solute fraction is available for bulk precipitation. However, the real reason may be more complicated as the conditions of precipitation heat treatment may also play a role. This phenomena should be studied in more detail.

Considering all three factors, in the ECAE at RT sample, initial structure is B2 and the M_s and M_f are below -60 °C because of heavy deformation and austenite stabilization. Annealing up to 600 °C in DSC led to a considerable increase in the TTs starting at the annealing temperature of 350 °C. TEM investigation of the annealed samples did not reveal any precipitation as presented in the following section. This may be an indication of either a lack of precipitates or formation of very small ones below the detection limit of the TEM (< 10 nm). Therefore, recovery and dislocation rearrangement should be responsible for the increase in TTs of the annealed ECAE @ RT samples, at least after low temperature annealing. When the samples are annealed at 600 °C for 30 minutes, the TTs are recovered to the level of the solutionized material.

In the case of the ECAE at 450 °C sample, the structure is B2 at room temperature, and the A_s and A_f are very close to that of the solutionized sample as shown in Figure 4.1.1 These temperatures are quite different than that of the samples which are solutionized and aged at 450 °C for 1 hour indicating that the precipitates were dissolved during the ECAE process which is also supported by TEM investigations presented subsequently. The M_s temperature is lower than that for the solutionized material due to austenite stabilization. However, the effect is not as pronounced as in the case of the

ECAE at RT sample showing that the microstructure should be partially recovered. Because of the partial recovery, the amount of increase in TTs after annealing above 300 °C is lower than that in the annealed ECAE at RT samples. Moreover, the A_f temperatures after different annealing temperatures are exactly the same as that of the sample solutionized and aged at 450 °C for 1 hour showing that the increase is not solely because of new precipitation as the effect of partially recovered deformed structure cannot be ignored.

Thus from calorimetric analysis we can conclude that SPD via ECAE led to suppression of transformability. The structure is found to be B2 austenite at room temperature.

4.2 Microstructural evolution after ECAE processing

Microstructural evolution after ECAE processing was done using TEM by comparing it with the initial microstructure before extrusion. In the solutionized material, a uniform microstructure with a grain size of approximately 60 microns is observed (Figure 4.2.1). Figure 4.2.2 (a) shows a bright field TEM image of the microstructure evolved after ECAE processing at RT. The microstructure is found to be a mixture of B2 austenite and B19' martensite as shown in the electron diffraction patterns (EDP) (Figures 4.2.2 (b) and 4.2.2 (c)). There is significant increase in the dislocation density as compared to the solutionized material (which is the starting condition) and neither grains nor grain boundaries can be distinguished in the TEM images. The rationale for these two observations is severe plastic deformation during ECAE processing (approximately 116% equivalent strain applied) which leads to strain hardening and suppression of the transformation temperatures to extremely low values. This explains the absence of transformation during annealing from -60 °C to 100 °C in DSC (Figure 4.1.1). The microstructure is composed of thick plates (approximately 300 – 400 nm) having thin plates inside (approximately < 50 nm) and looks like a typical martensite morphology; however, interestingly, the B2 phase is evident from the EDP and it is the main phase. The initial deformation mechanism of this alloy at room temperature is stress-induced martensitic transformation (SIM) followed by detwinning and plastic deformation of the

martensite via dislocation slip or deformation twinning [41]. Therefore, martensite should be the main phase present in this material after deformation unless there is a back transformation upon unloading (pseudoelasticity). Pseudoelasticity, on the other hand, may not be possible because if the material is heavily deformed in martensite (i.e. marformed), martensite stabilization usually occurs [37].

Although martensite was expected, the B2 phase is the main phase observed. There might be three possible mechanisms to explain the unusual observation of the B2 phase in our case: 1) deformation heating leading to partial back transformation; 2) deformation heating that causes B2 to deform with mechanical twinning resulting in the well-organized structure observed in Figure 4.2.2, and 3) initially stress induced martensite (SIM) takes place and it transforms into B2 after (or during) processing. Since the extrusion rate is very low, deformation heating as much as would be necessary to increase the temperature above M_d (highest temperature at which SIM is observed) is not expected. Therefore, the second mechanism may not be feasible. Since the morphology of the B2 phase observed in figure 4.2.2 is similar to the martensite variant and the internal twin structure in appearance, the responsible mechanism should involve SIM and a subsequent $B19' \rightarrow B2$ transformation either via thermally induced back transformation or back transformation by some other means. Figure 4.2.3 shows a schematic of the proposed mechanism of the deformation twin formation in B2 austenite during severe plastic deformation of 50.8 at % NiTi below M_d temperature via a $B2 \xrightarrow{\text{SIM}} B19' \xrightarrow{\text{SPD}} B2$ transformation sequence.

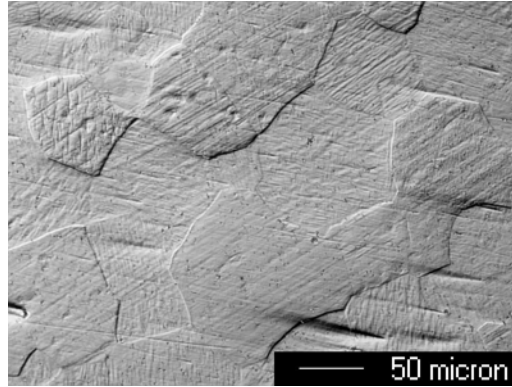


Figure 4.2.1 Optical micrograph of solutionized 50.8 at % NiTi material with a grain size of about 60 microns.

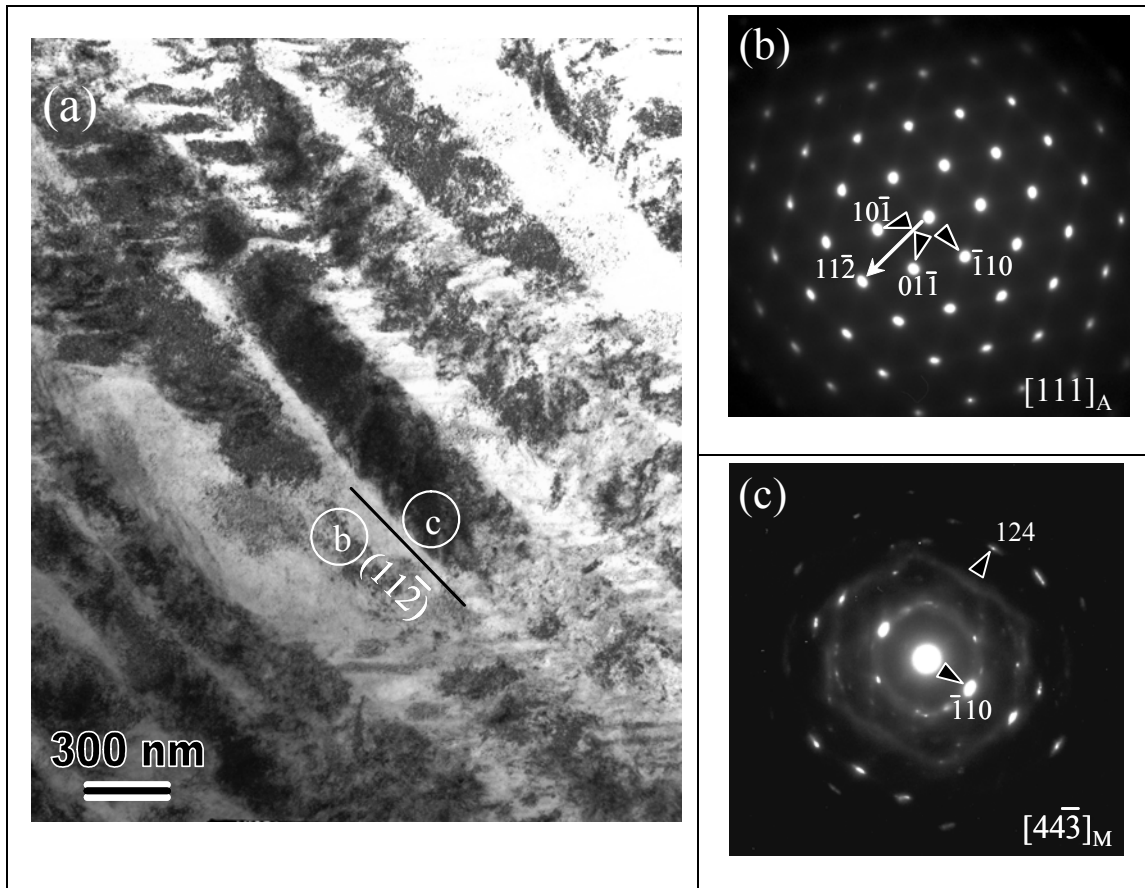


Figure 4.2.2 (a) Bright field TEM image of 50.8 at. % NiTi ECAE processed at RT. The sample contains mainly B2 and B19' phases. The EDP in (b) is taken from the circled area which is indexed as the B2 phase along the $[111]$ direction. The twinning plane trace in the image (a) is perpendicular to the vector $(11\bar{2})_{B2}$, which implies that the twinning plane is $(11\bar{2})_{B2}$ as marked. The EDP from a single martensite lath in (c) shows the B19' structure.

Figure 4.2.4 shows (a) bright field, (b) dark field and (c) dark field TEM images of 50.8 at % NiTi ECAE at RT material. Twins are observed inside twins.

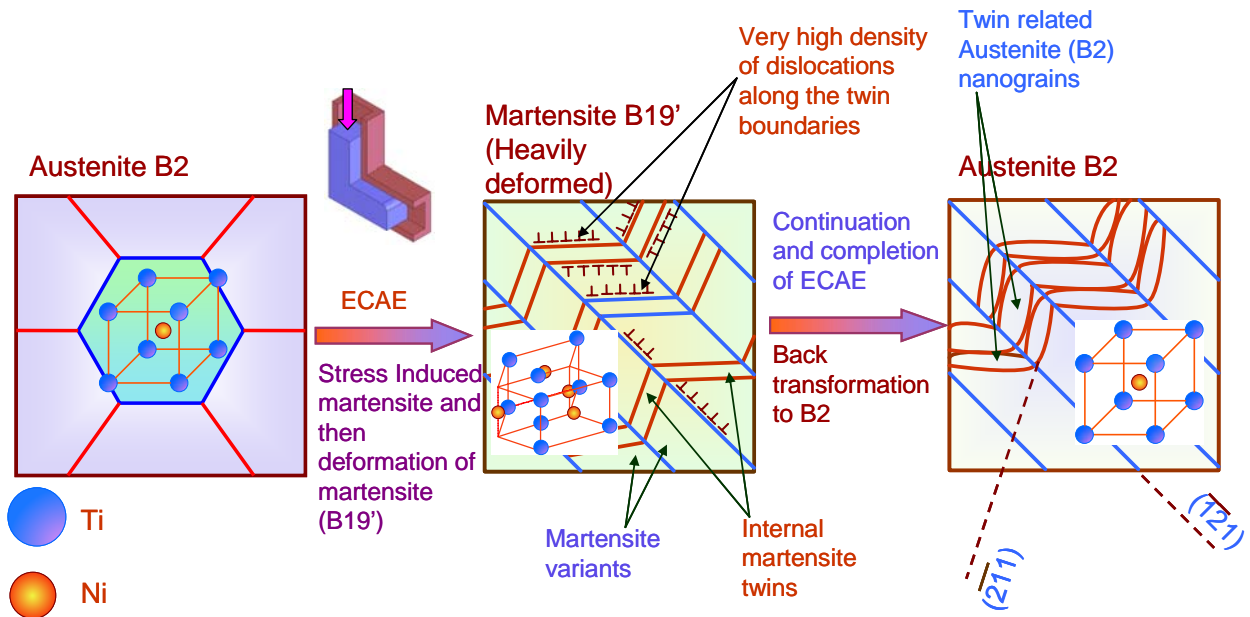


Figure 4.2.3 A schematic of the proposed mechanism of the deformation twin formation in B2 austenite during severe plastic deformation of 50.8 at % NiTi below M_d temperature via $B2 \xrightarrow{\text{SIM}} B19' \xrightarrow{\text{SPD}} B2$ transformation sequence.

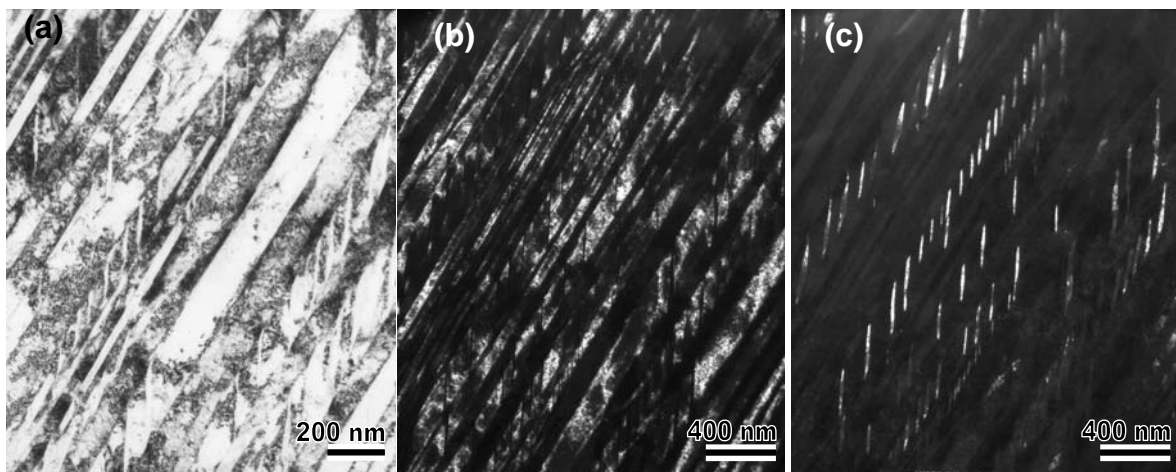


Figure 4.2.4 (a) Bright field, (b) dark field and (c) dark field TEM images of 50.8 at % NiTi ECAE at RT.

The aging of solutionized material at 450 °C for one hr led to the formation of incoherent Ni_4Ti_3 precipitates (four variants) with the size of about 200-250 nm (Figure 4.2.5 (d)). This is the starting microstructure for ECAE at 450 °C extrusion. Figure 4.2.5 (a) shows microstructure evolved after extrusion at 450 °C. Both the B19' martensite and the B2 austenite are observed with occasional recrystallized nanograins. The unique micro structural observations include the absence of precipitates which were present before extrusion (Figure 4.2.5 (d)), an increase in dislocation density, and grain refinement although the grain boundaries are poorly defined. The maximum size of the grains is about 200-250 nm. A possible explanation for the absence of precipitates after ECAE processing is cutting of particles by dislocations during extrusion. The diffraction contrast is not uniform due to high localized distortion. Note that 450 °C is well above A_f , and there is no report of a SIM transformation at temperatures this high, as the M_d temperature of NiTi alloys is usually less than 200 °C [41]. The observed martensite should be either strain induced or could be formed during cooling to room temperature. The latter, however, is not a reasonable assumption because austenite stabilization occurs during ausforming and M_s is suppressed as shown by the DSC results (Figure 4.1.1).

Therefore, this is the first study in which a strain induced martensitic transformation is observed in NiTi. Although distinctive R-phase peaks are not observed in the DSC response of as-processed ECAE at 450 °C samples (Figure 4.1.1), the EDP in Figure 4.2.5 (c) shows the existence of weak reflections along the $1/3\{101\}_{\text{B2}}$ positions that specify the R-phase. The presence of R-phase indicates some recovery during ECAE processing at 450 °C, since the R-phase is not expected in heavily deformed structures as was the case for the ECAE at RT material.

Figure 4.2.6 shows (a) bright field and (b) dark field TEM images of the ECAE at 450 °C material. A small volume fraction of deformation twins are observed along with nanocrystallized grains. Although the volume fraction of twins was less as compared to the ECAE at RT material (Figure 4.2.2 and Figure 4.2.4), the twins were longer in length.

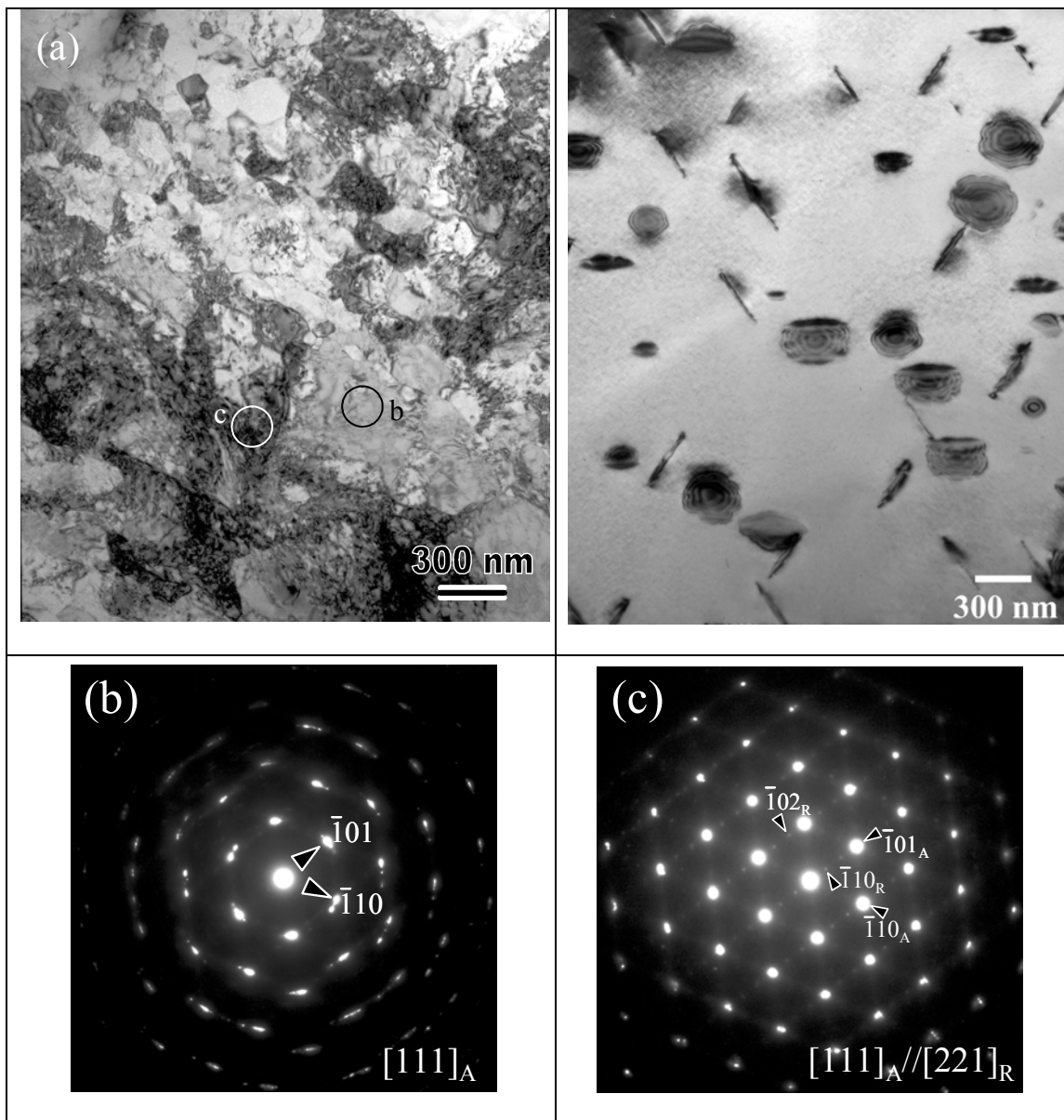


Figure 4.2.5 (a) Bright field TEM image of 50.8 at % NiTi ECAE processed at 450 °C. The EDP in (b) shows B2 phase structure along the $[111]$ direction. In the EDP of (c), a close inspection shows the existence of weak reflections along the $\frac{1}{3}\{101\}_{B2}$ positions that indicate the R phase. (d) solutionized + aged material at 450 °C for 1 hour which

shows the starting microstructure of ECAE @ 450 °C sample. Four variants of Ni_4Ti_3 precipitates are evident.

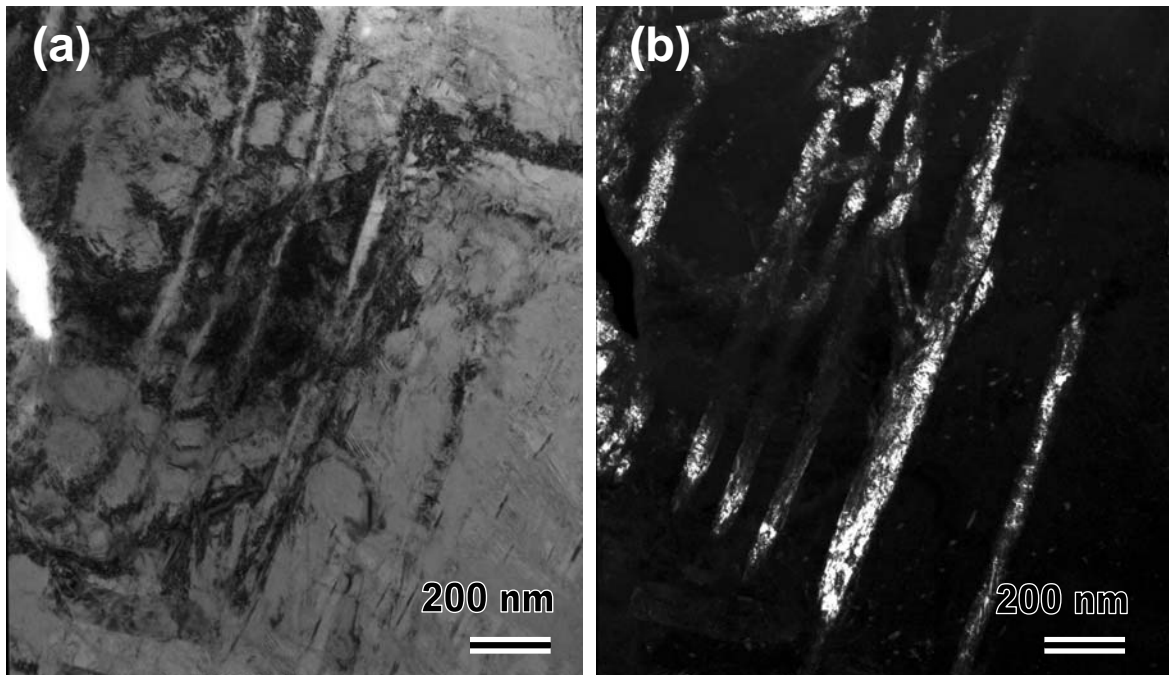


Figure 4.2.6 (a) Bright field, (b) dark field TEM images of 50.8 at % NiTi ECAE at 450 °C.

4.3 Microstructural observation in annealed material after ECAE processing

ECAE at RT material was annealed at 450°C for 30 min and TEM was conducted on resulting microstructure. Figures 4.3.1 (a) and 4.3.1 (b) show the bright and dark field TEM images, respectively, of the microstructure after annealing of the ECAE at RT sample at 450°C for 30 min. There is a considerable reduction in dislocation density with the enlargement of thin plates observed in Figure 4.2.2 (a), forming more ellipsoidal grains. The size of these grains was found to be about 100 nm along the minor axis. These nanograins are twin-related as shown in Figures 4.3.1 (c) and 4.3.1 (d), similar to what was observed in Figure 4.2.2 (a) with the same twinning planes (i.e. $\{11\bar{2}\}$). The dark field image in Figure 4.3.1 (b) was taken from the $(12\bar{1})_T$ reflection illustrating the twin relation. The EDP in Figure 4.3.1 (c) was taken from the big circled area, marked as “c” in Figure 4.3.1 (a), which shows the reflections from both the matrix and twins. The EDP in Figure 4.3.1 (d) was taken using a very small aperture from the circled area marked as “d” in Figure 4.3.1 (a), showing the only reflections of the twins. The twinning plane is identified as $(\bar{2}\bar{1}1)$, as evidenced from the fact that the vector $\mathbf{g}_{(\bar{2}\bar{1}1)}$ is perpendicular to the trace of the horizontal twins. Note that there is another twinning plane $(\bar{1}\bar{2}1)$, with the vector $\mathbf{g}_{(\bar{1}\bar{2}1)}$ perpendicular to the trace of the twin planes. The angle between these two twinning planes is measured as 34°, which is close to the calculated one of 33.5°. Again the twin planes were found to be $\{112\}_{B2}$ type and the arrangement of nanograins stayed the same without fragmentation or reorientation during recovery. Figure 4.3.2 shows more TEM images and corresponding diffraction patterns for ECAE at RT after annealing at 450 °C for 30min.

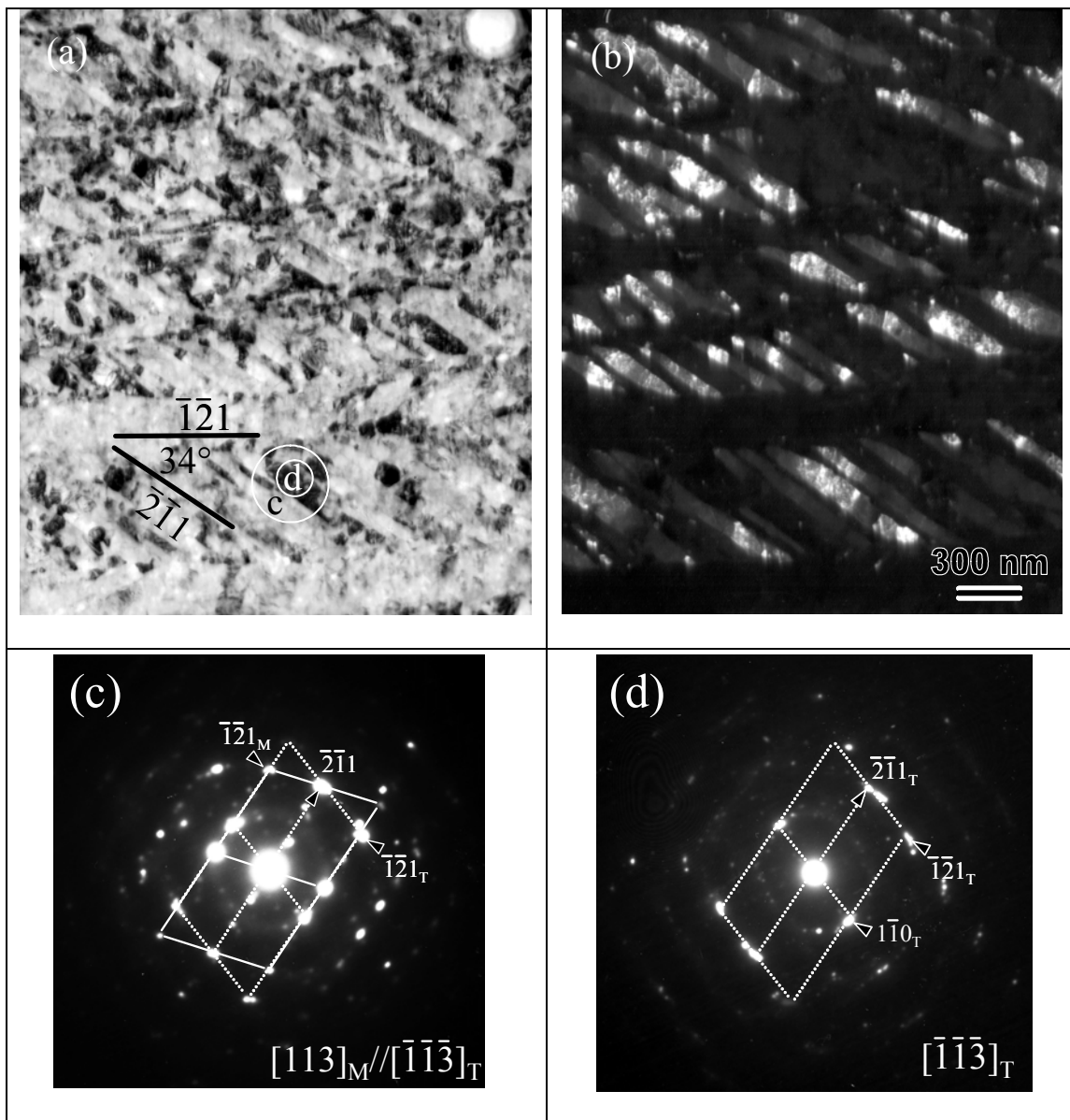


Figure 4.3.1 (a) Bright and (b) dark field TEM images of ECAE at RT sample annealed at 450°C for 30 min, demonstrating twin related nanograins in B2 austenite. (c) and (d) show the electron diffraction patterns taken from the circled areas shown in (a). The dark field image in (b) was taken from the $(12\bar{1})_T$ reflection showing the twin related grains. Please note that no precipitates were observed after annealing at 450°C for 30 min in support of the arguments in Section 4.1 for describing the increase in TTs.

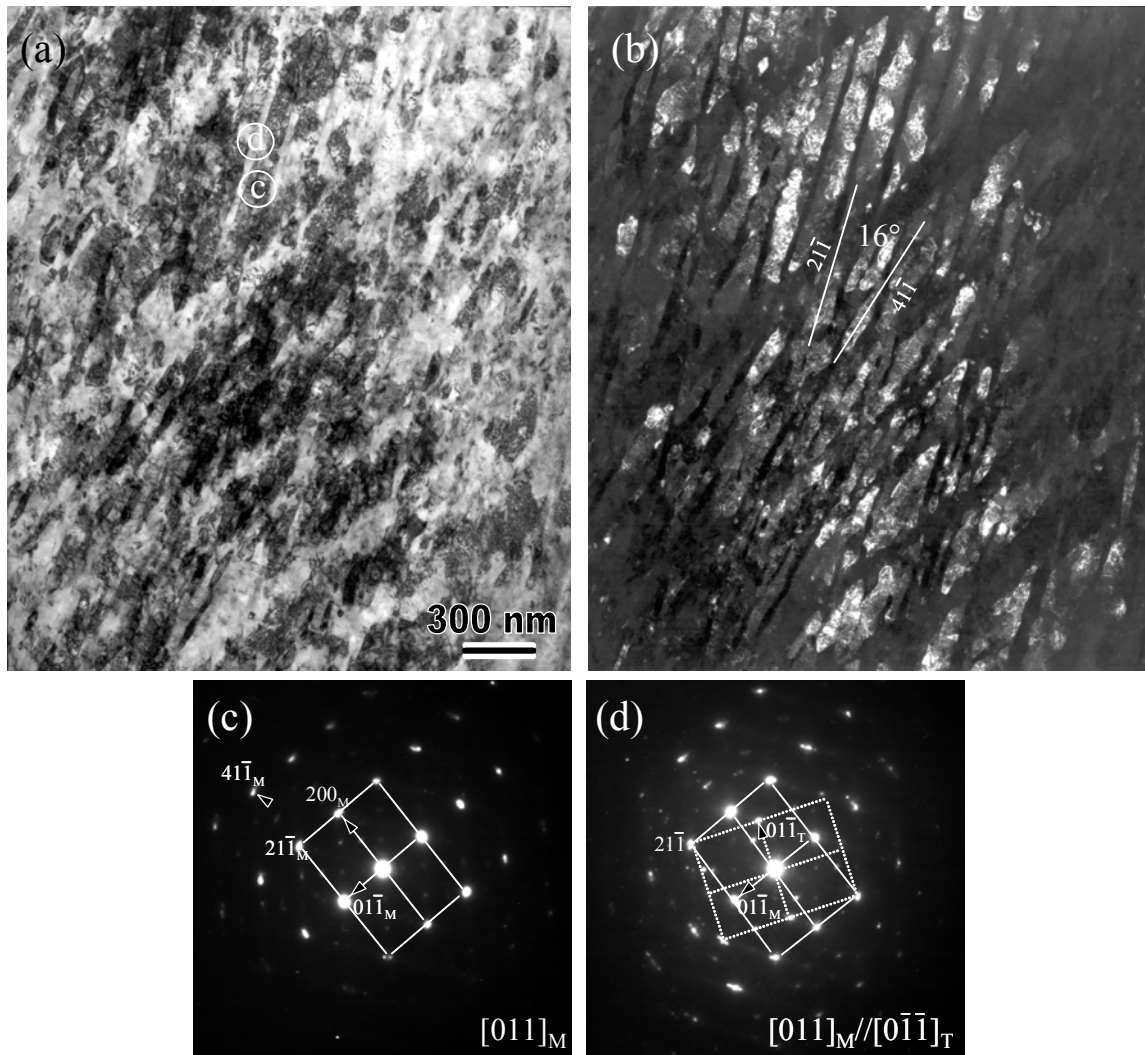


Figure 4.3.2 (a) Bright and (b) dark field TEM images of ECAE at RT sample annealed at 450°C for 30 min, demonstrating twin related nanograins in B2 austenite. The dark field image in (b) is taken by the $(0\ 1\ -1)_M$ reflection. The EDP in Fig. (c) is taken from the circled area marked as “c” in Fig. (a). The EDP in Fig. (d) is taken from the circle marked as “d” in Fig. (a), showing the reflections of both matrix and twins. Note there is a secondary plane trace with angle of 16° apart away from $(2\ 1\ -1)$, which is identified as $(4\ 1\ -1)$ which trace is perpendicular to the $g(4\ 1\ -1)$ vector.

Figures 4.3.3 and 4.3.4 show the bright field TEM images of the ECAE at RT material after annealing at 600 °C and 700 °C for 30 minutes, respectively. Complete recovery and recrystallization has occurred with considerable grain growth. The grains are no longer twin related as in the case of a 450°C - 30 min heat treatment (Figures 4.3.1 and 4.3.2). Thus the twin related grain morphology is dissolved and equiaxed grains are seen to nucleate after a 600 °C - 30 min heat treatment. A non uniform grain size distribution was observed in the 600 °C – 30 min heat treated sample with grain size ranging from 200 nm to 3 μm, whereas the 700 °C - 30min heat treatment resulted in uniform grain size of 25 μm. Both heat treatments did not result in any detectable precipitates.

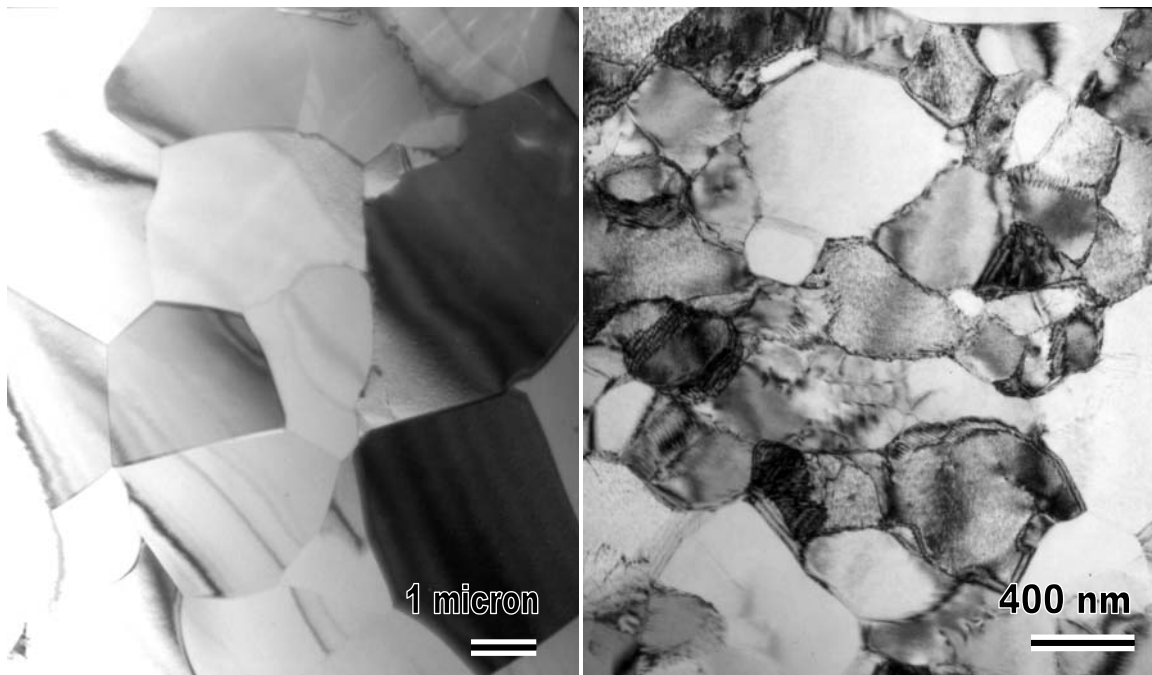


Figure 4.3.3 Bright field TEM images of ECAE at RT material after annealing at 600 °C for 30 minutes.

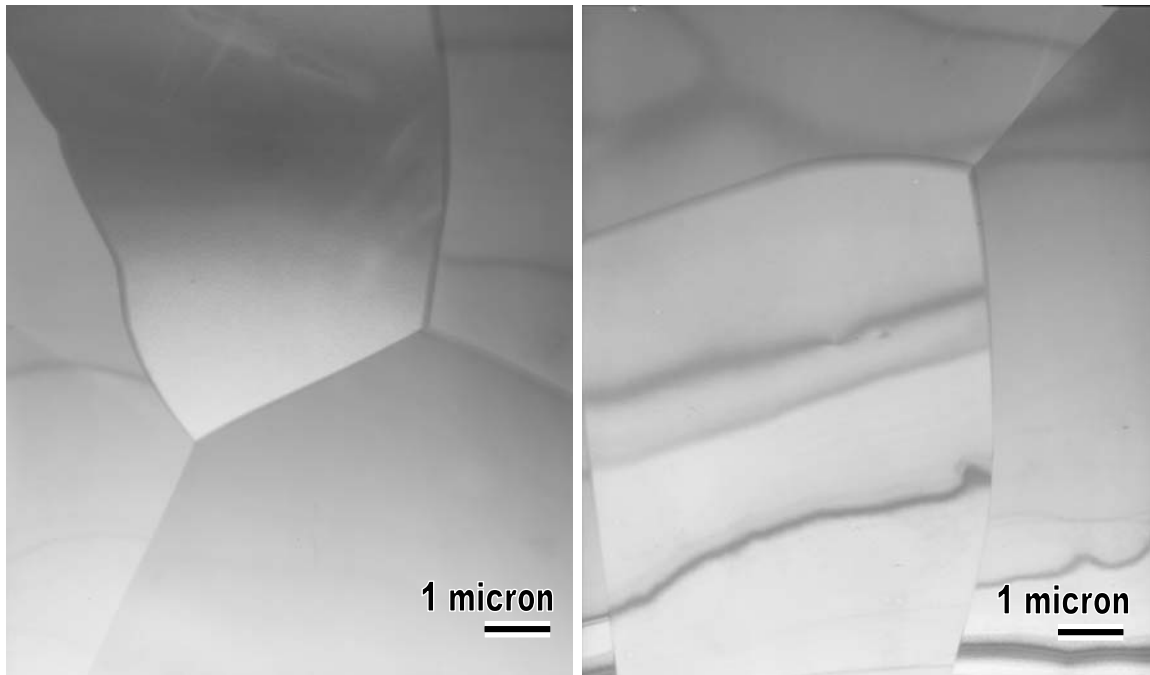


Figure 4.3.4 Bright field TEM images of ECAE at RT material after annealing at 700 °C for 30 minutes.

The conservation of twin related morphology upon low temperature annealing is a unique finding because this may open a new opportunity for twinning induced grain boundary engineering in NiTi alloys. The methodology would create nanostructured materials with low correspondent site lattice (CSL) grain boundaries. It is believed that the well-organized microstructure with nanostructured grains would improve the cyclic stability of these materials because of the strengthening of the B2 phase. This may also have some implications for the fracture mechanisms of NiTi alloys.

Figure 4.3.5 shows the effect of annealing temperature on grain size for the ECAE at RT material. There is a gradual increase in the grain size of the material up to 600 °C, after which it increases rapidly. Therefore, the recovery occurs up to 500-600 °C and rapid recrystallization and grain growth starts after 600 °C.

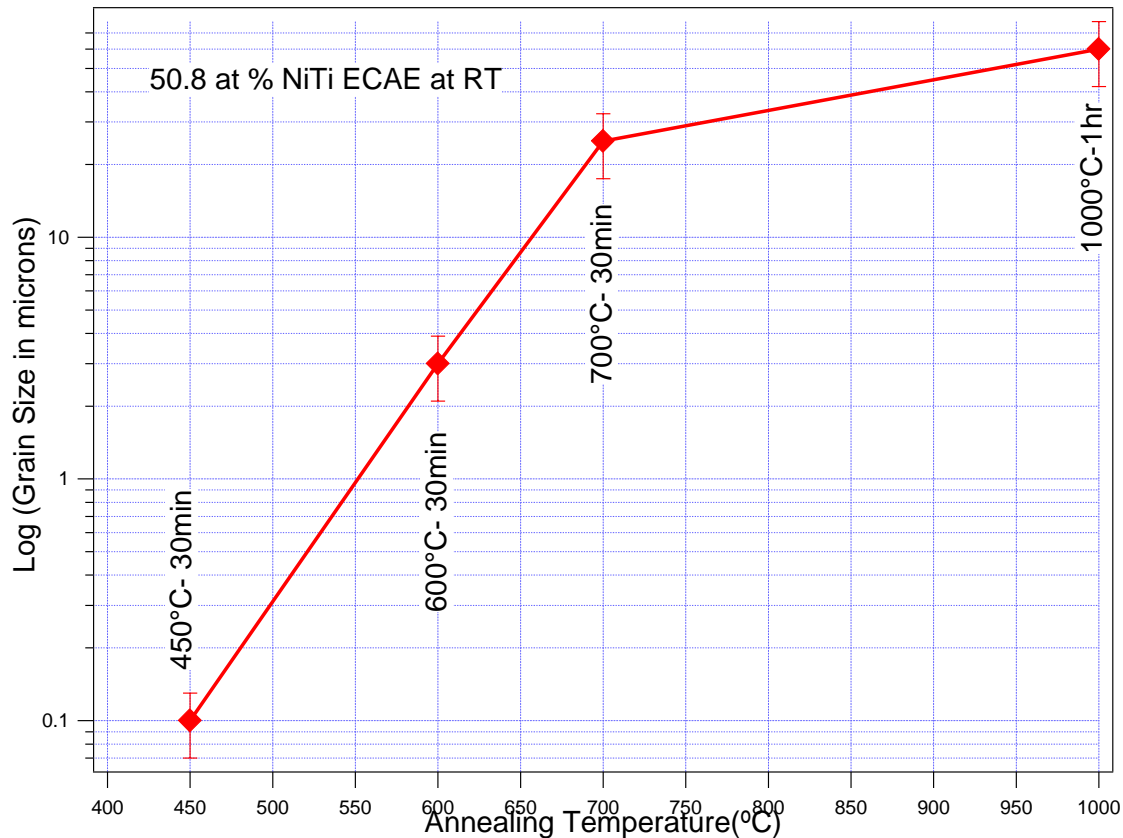


Figure 4.3.5 Effect of annealing temperature on the grain size of ECAE at RT material.

Figure 4.3.6 shows the effect of grain size on temperature hysteresis (A_f - M_s) for the ECAE at RT material after different annealing treatments. The hysteresis is extremely high (100 °C) at 450 °C for a 30 min heat treatment, but it drops suddenly to 23 °C at a 600 °C – 30 min heat treatment and remains 19 °C thereafter. This behavior can be correlated to TEM observations, as seen in bright and dark field TEM images of ECAE at RT 450 °C for 30 min annealed material (Figures 4.3.1 and 4.3.2). Nano grains (grain size ~100 nm along minor axis), a high dislocation density and deformation twins are observed compared to a dislocation and deformation twin free microstructure with large grains in 600 °C for 30 min and 700 °C for 30 min annealed material in Figures 4.3.3 and 4.3.4, respectively. These dislocation structures and deformation twins along with nano grains form a complex network which offers a high resistance to the austenite-martensite

interface motion and thus increases the thermal energy required for the transformation i.e. hysteresis (A_f-M_s). Also note that there is not much difference in the hysteresis values for 600 °C, 700 °C and solutionized material since 600 °C for 30 min heat treatment led to complete recrystallization.

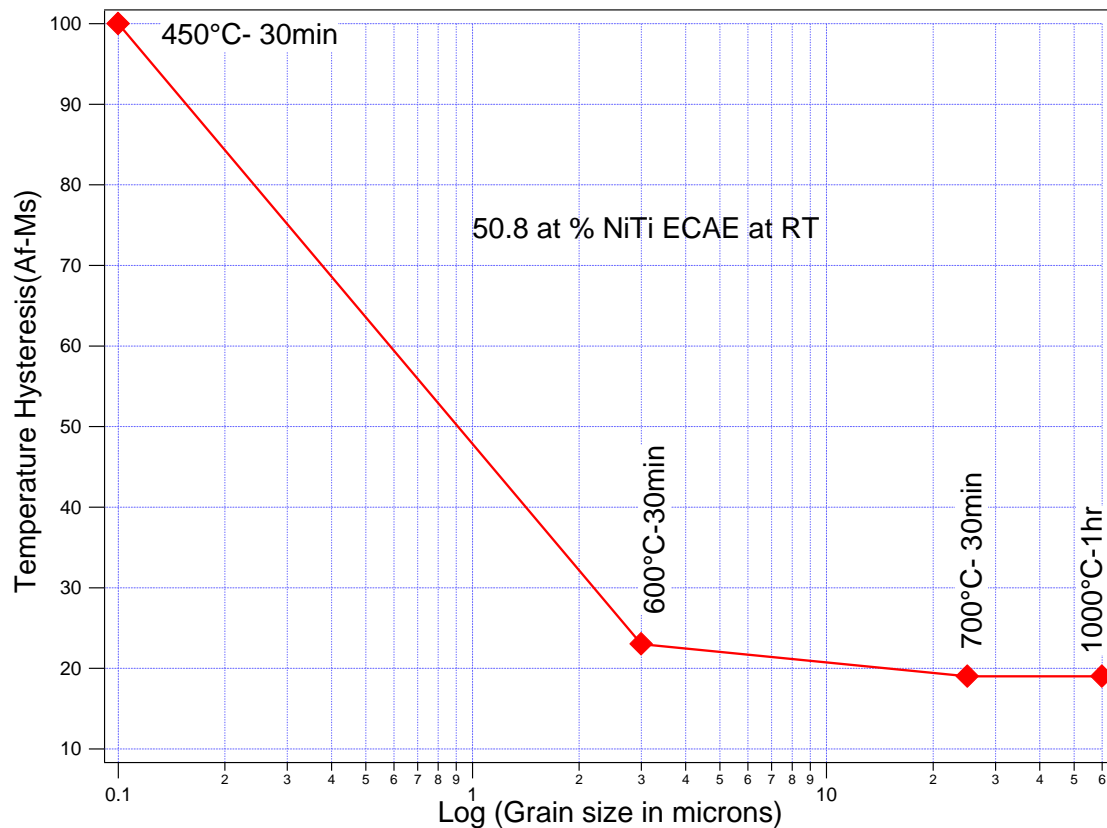
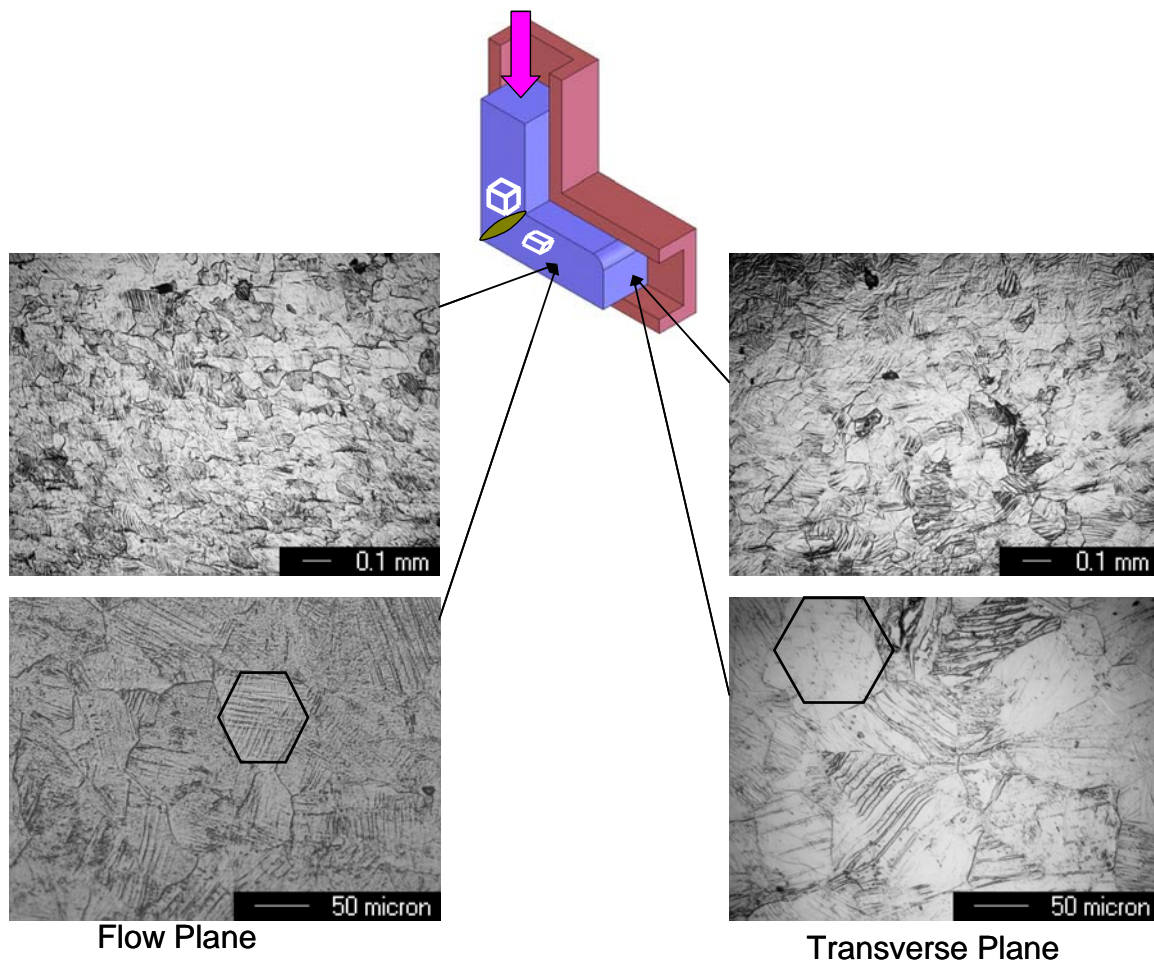


Figure 4.3.6 Effect of grain size on temperature hysteresis for the ECAE at RT material after different annealing treatments.

Figure 4.3.7 shows the optical micrograph of 50.7 at % NiTi after extrusion at 450 °C using route 1A (Figure 4.3.7 (a)) and route 2C (Figure 4.3.7 (b)). The effect of extrusion on grain morphology and grain refinement is more pronounced in the case of route 2C than in route 1A. The grain morphology shows that the grains are equi-axed

along the transverse plane for both routes. Along the flow plane the grains are elongated in the case of route 2C, but they remain equi-axed for route 1A.



(a)

Figure 4.3.7 Optical micrograph of 50.7 at % NiTi after (a) ECAE at 450 °C 1A route, and (b) ECAE at 450 °C 2C route.

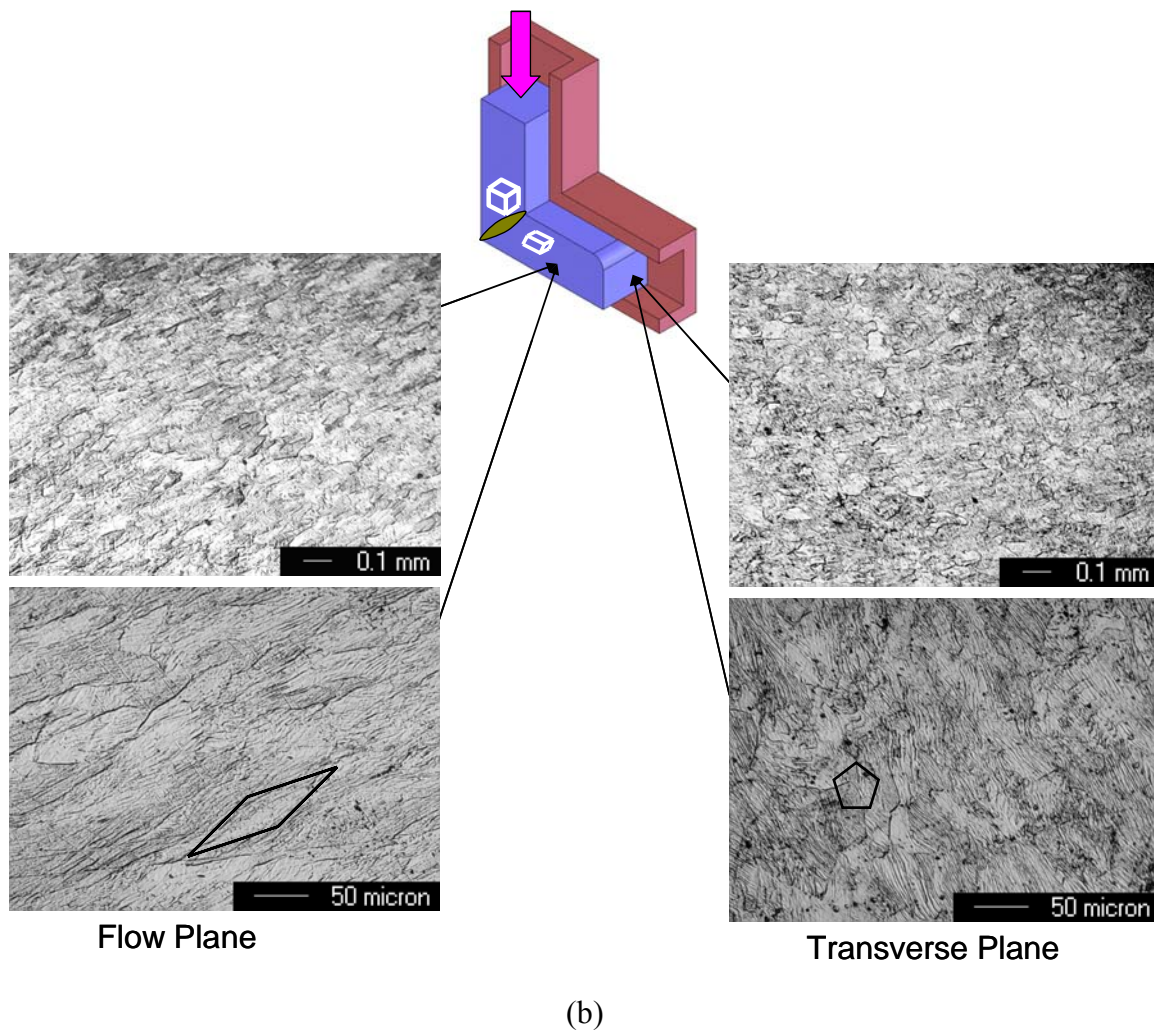


Figure 4.3.7 Continued.

Thus from microstructural investigation we can conclude that SPD via ECAE led to grain size refinement and introduction of dislocation substructure. Upon low temperature annealing heat treatment of ECAE at RT material led to nucleation of twin related well organized nanocrystals.

4.4 Mechanical properties

a. Incremental straining

Figure 4.4.1 shows the response of (a) as-received, (b) solutionized, (c) as-received and annealed at 450°C for one hr, (d) solutionized and aged at 450°C for one hr and (e) ECAE at 450°C during the incremental straining in compression at a temperature of $A_f + 20^\circ\text{C}$. Experiments were conducted in the austenitic state at $A_f + 20^\circ\text{C}$, where martensite is unstable and pseudoelasticity (PE) is ensured. Diamond shaped markers and the scale on the right hand axis shows the pseudoelastic (PE) recoverable strain in percentage. Please refer to Figure 1.1.4 for the description of the PE recoverable strain. The main goal of these experiments was to find out the stress required for inducing martensite, the yield stress for martensite (start of second plateau), the maximum strain level at which the transformation is purely a stress induced martensitic transformation without moving into the elastic region of martensite, and PE recoverable strain. The stress for inducing martensite is a function of temperature given by the Clausius–Clapeyron relationship [23] and increases with increasing temperature. Ideally the stress for inducing martensite is zero at the M_s temperature because the transformation starts by thermal activation. Therefore, the experiments were conducted at the same temperature ($A_f + 20^\circ\text{C}$). Also, a low ratio of stress for inducing martensite to the yield stress is considered as a prerequisite for stable cyclic response [23].

As-received material (Figure 4.4.1.a) was strained up to 4% strain in compression, but continuous hardening was observed. Usually the plateau region is observed during the stress induced martensitic transformation, but it was not observed in this sample. This is due to the fact that during cold working there is a partial loss of transformability because of a high density of dislocations which act as a barrier to the austenite-martensite interface motion and suppresses transformability [31,32]. Therefore the sample was not further strained.

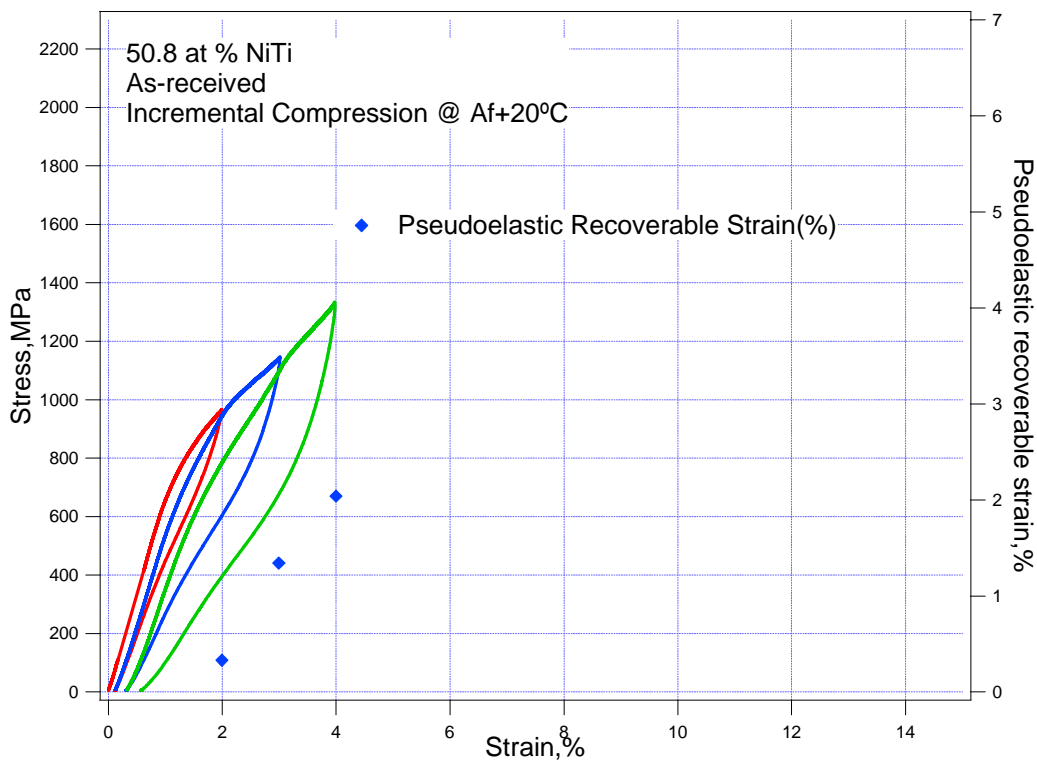


Figure 4.4.1.a Incremental strain response under compression of as-received material.

Figure 4.4.1.b shows the incremental strain response of solutionized material. Pseudoelasticity (PE) is observed with a plateau region during the stress induced martensitic transformation unlike the as-received material. However, large irrecoverable strains upon unloading are accumulated due to dislocation generation during the austenite-martensite interface motion [25]. Since the matrix is soft in the solutionized material, dislocation generation is easier, leading to high irrecoverable strains and lower yield strength (1010 MPa).

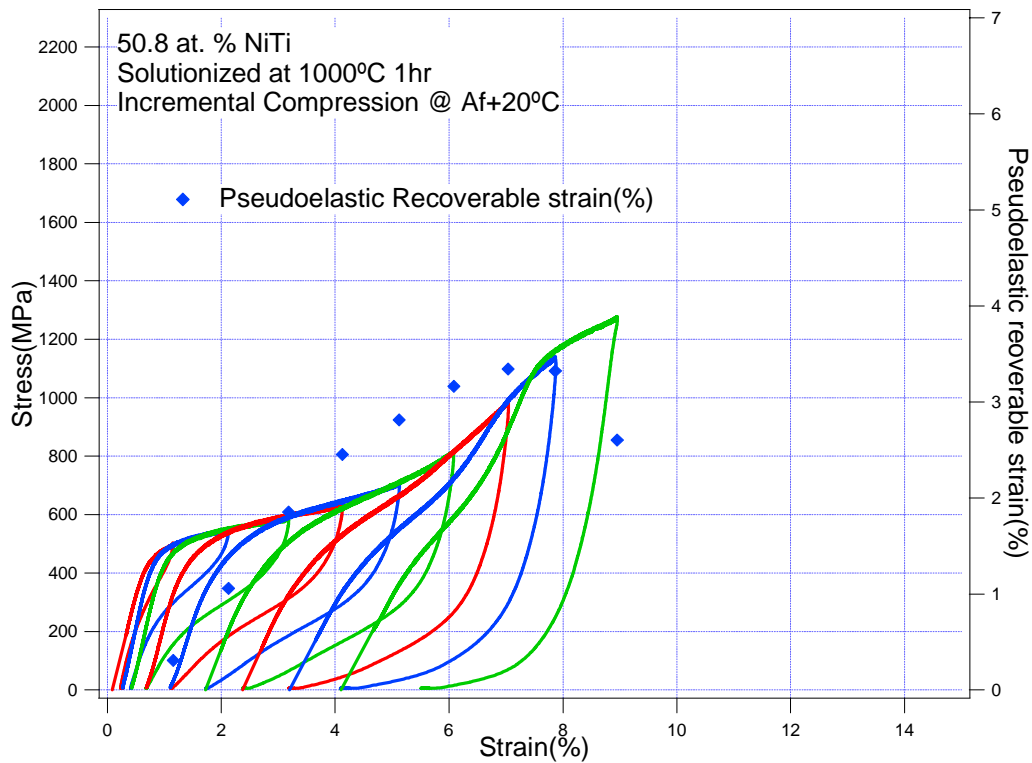


Figure 4.4.1.b Incremental strain response under compression of solutionized material.

Figure 4.4.1.c shows the incremental strain response of as-received material after annealing at 450°C for one hr. Partial pseudoelasticity with a plateau region during the stress induced martensitic transformation is observed in this material which was not present before annealing (Figure 4.4.1.a). A low temperature annealing heat treatment led to partial recovery and recrystallization [31,32] while preserving the high yield strength to 1620 MPa.

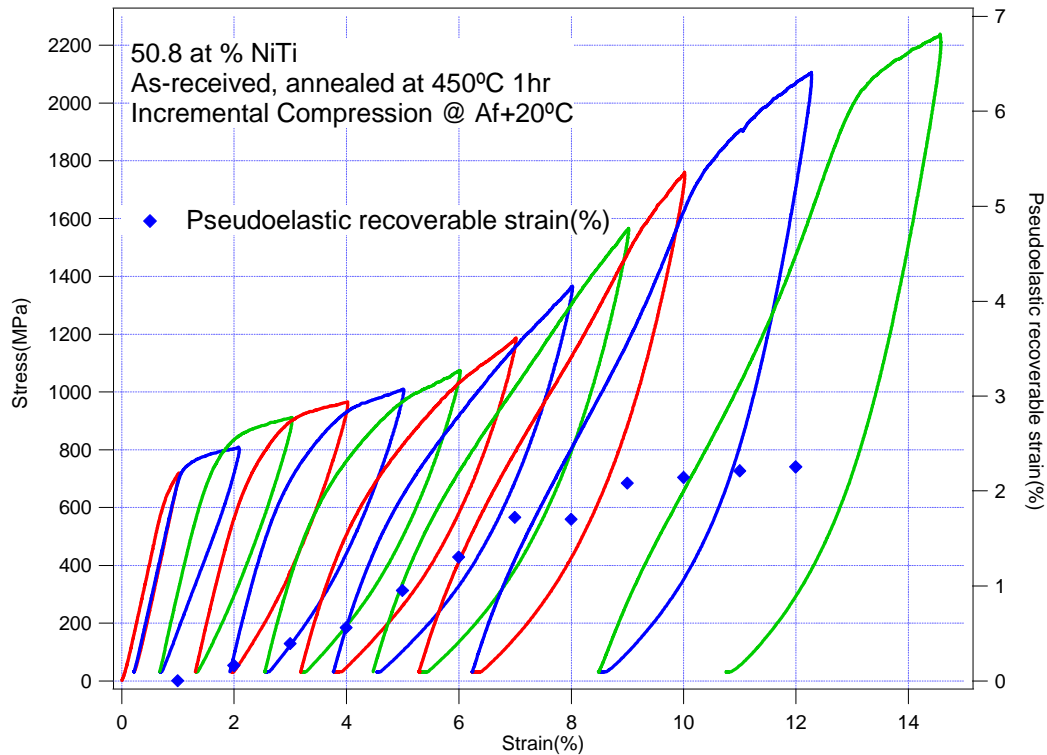


Figure 4.4.1.c Incremental strain response under compression of as received + annealed at 450°C for 1hr. material.

Figure 4.4.1.d shows the incremental strain loading response for the solutionized material after aging at 450°C for one hr. Aging leads to the nucleation of Ni_4Ti_3 incoherent precipitates (four variants) with a precipitate size of about 200-250 nm (Figure 4.2.3 (d)). The transformation stress for aged material (550 MPa) is higher by 50 MPa than for solutionized material (500 MPa). Usually, peak aging leads to nucleation of fine coherent precipitates [36]. These fine coherent precipitates assist the transformation (nucleation of martensite crystals) by strong local stress fields around them and decrease the transformation stress level. However, over aging (450°C for one hr) produced coarse incoherent precipitates which lost coherency with the matrix and thus did not assist the transformation. No pseudoelasticity (PE) was observed in this material which was present

before aging (Figure 4.4.1.b) due to the high volume fraction of precipitates which are unable to undergo transformation [36] and possibly due to lack of internal local stress to bias martensite variant formation.

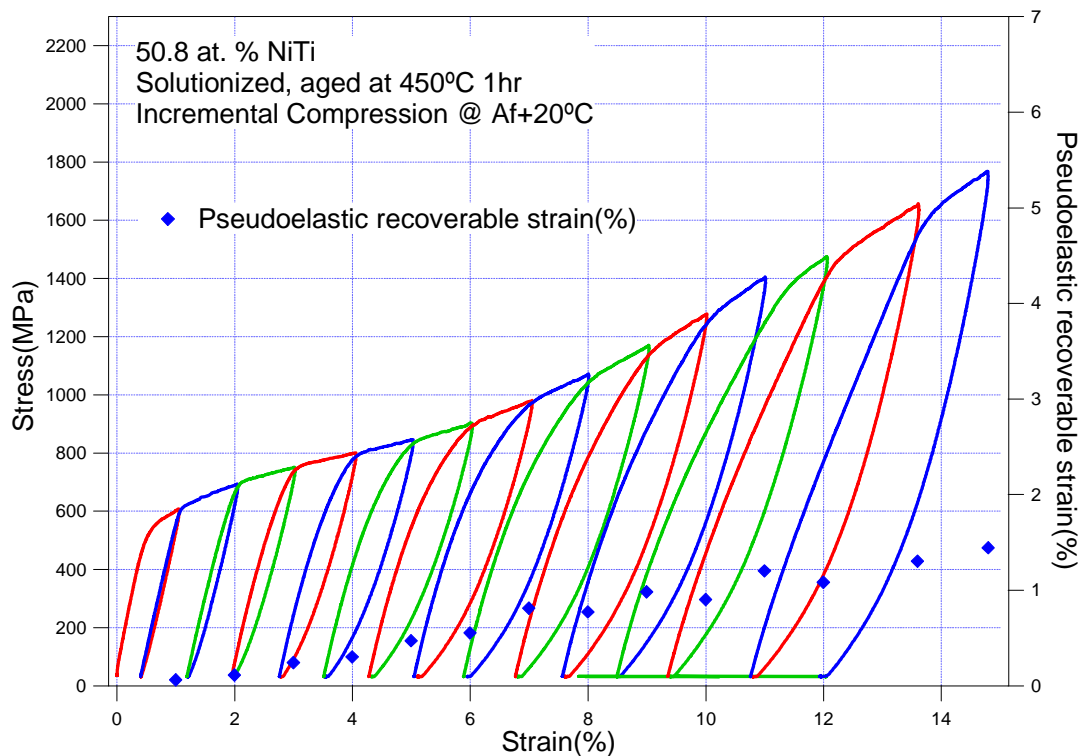


Figure 4.4.1.d Incremental strain response under compression of solutionized + aged at 450°C for 1hr material.

Figure 4.4.1.e shows the incremental strain response for the material ECAE processed at 450°C. It is noteworthy to observe ~0% irrecoverable strain for 4% applied strain. Also the values of irrecoverable strain at higher applied strain levels are lowest among the other deformation and heat treatment conditions (Figures 4.4.1.a-4.4.1.d).

There is also considerable increase in the yield strength (by about 610 MPa) as compared to solutionized (Figure 4.4.1.b). The strengthening mechanism for ECAE processed material is microstructural refinement and introduction of dislocation substructures (relatively high dislocation density) as shown in Figure 4.2.4.

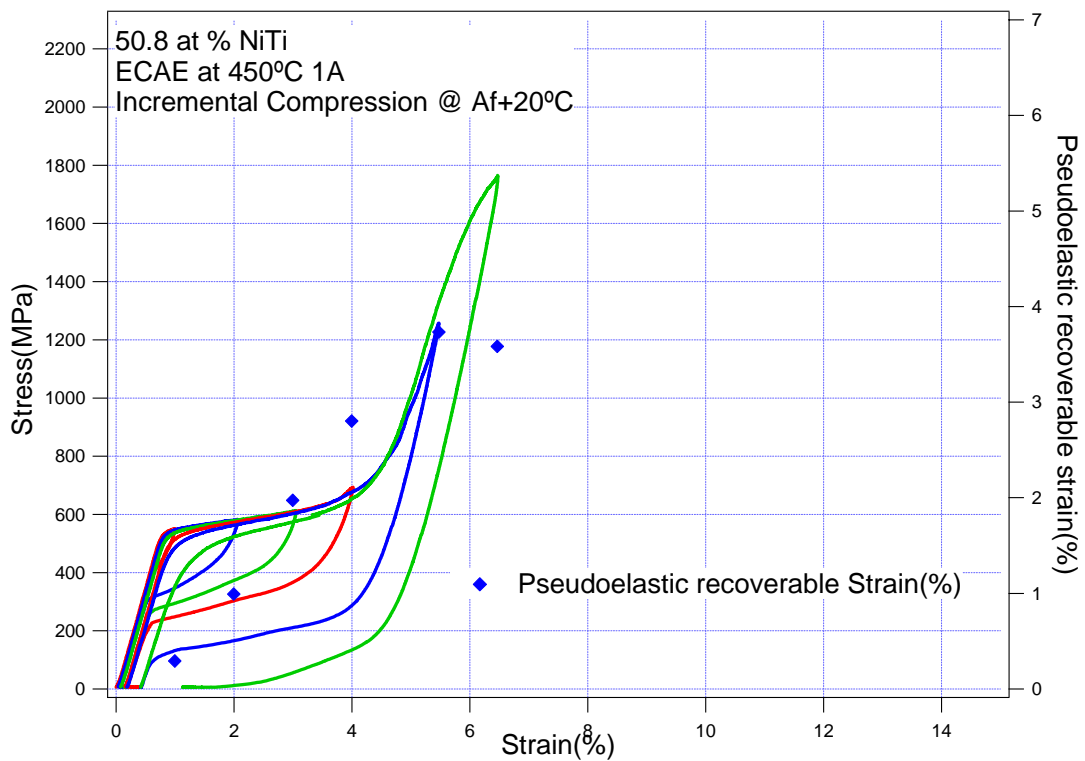


Figure 4.4.1.e Incremental strain response under compression of ECAE at 450°C material.

Although the yield strength for the as-received material after annealing (1620 MPa) is same as the ECAE processed material, the stress for inducing the martensitic transformation is higher for the as-received material after annealing (700 MPa) than for

the ECAE processed material (525 MPa). Therefore, the ratio of stress for inducing martensite to yield stress, for the ECAE processed material (0.32) is lower than the as-received material after annealing (0.43) and the solutionized material (0.49). A low ratio of stress for inducing martensite to yield strength of martensite (second plateau) ensures a higher strength material while preserving the transformation at lower stress levels without the introduction of significant defects (along martensite - austenite interface) which are the prerequisites for a stable cyclic response. Thus, the ECAE processed sample proves to be the most promising candidate for stable cyclic response.

b. Thermal cycling response under stress

As-received, as-received and annealed at 350°C for 30min, as-received and annealed at 450°C for one hr, solutionized, solutionized and aged at 400°C for 30min and ECAE processed at 450°C compression samples were thermally cycled between a temperature below M_f and a temperature above A_f , usually between -120°C and 200°C, at various stress levels.

Figure 4.4.2 explains the definition of transformation strain, creep strain, and thermal hysteresis on a typical strain-temperature curve of a shape memory alloy thermally cycled under stress. The main goal of these experiments is to investigate the stress dependence of thermal hysteresis, determine the transformation strain and construct a Clausius–Clapeyron curve. During thermal cycling, defects are introduced in the matrix at the austenite-martensite interface as discussed previously [25] in the case of a soft matrix, and these defects increase the dissipation energy thus increasing the thermal hysteresis [48]. In short, more and more heating/cooling is required (for the motion of interface) to provide enough thermal energy to compensate the elastic energy dissipation and to overcome the barrier against austenite/martensite interface motion. This additional energy is provided by undercooling during forward transformation and overheating during reverse transformation.

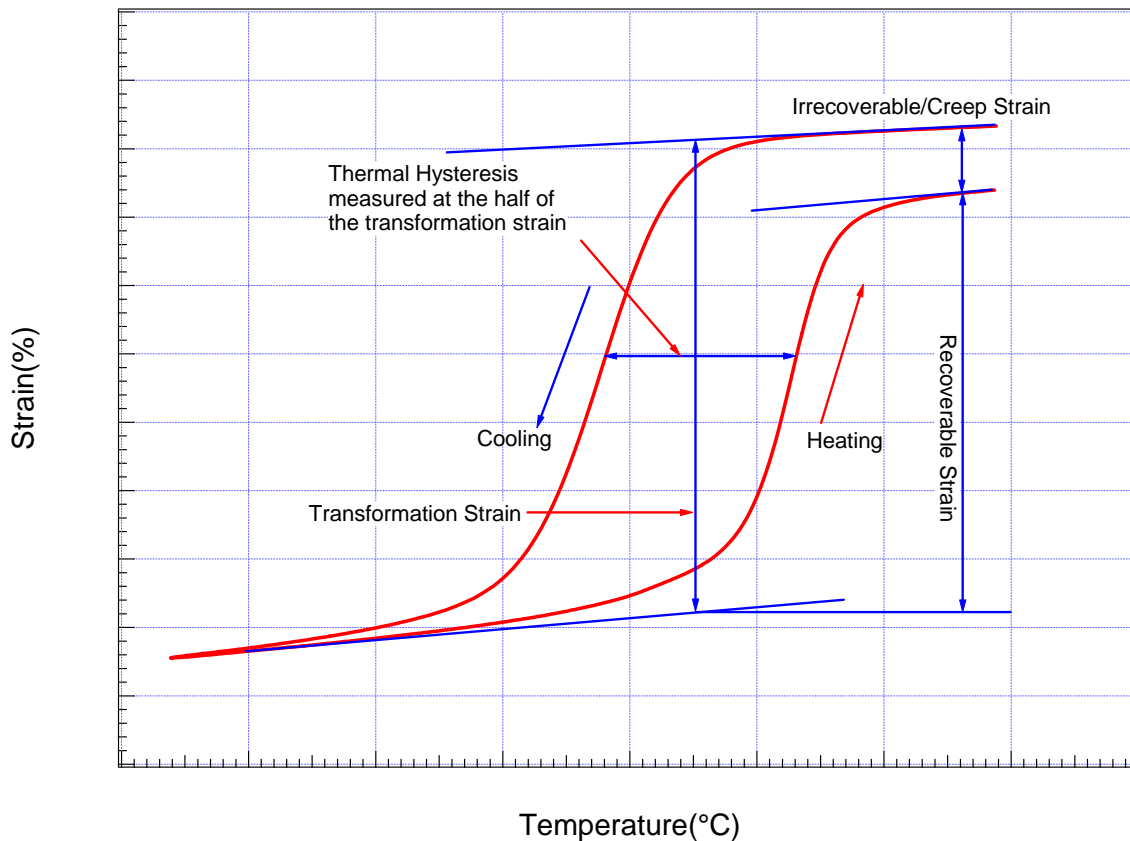
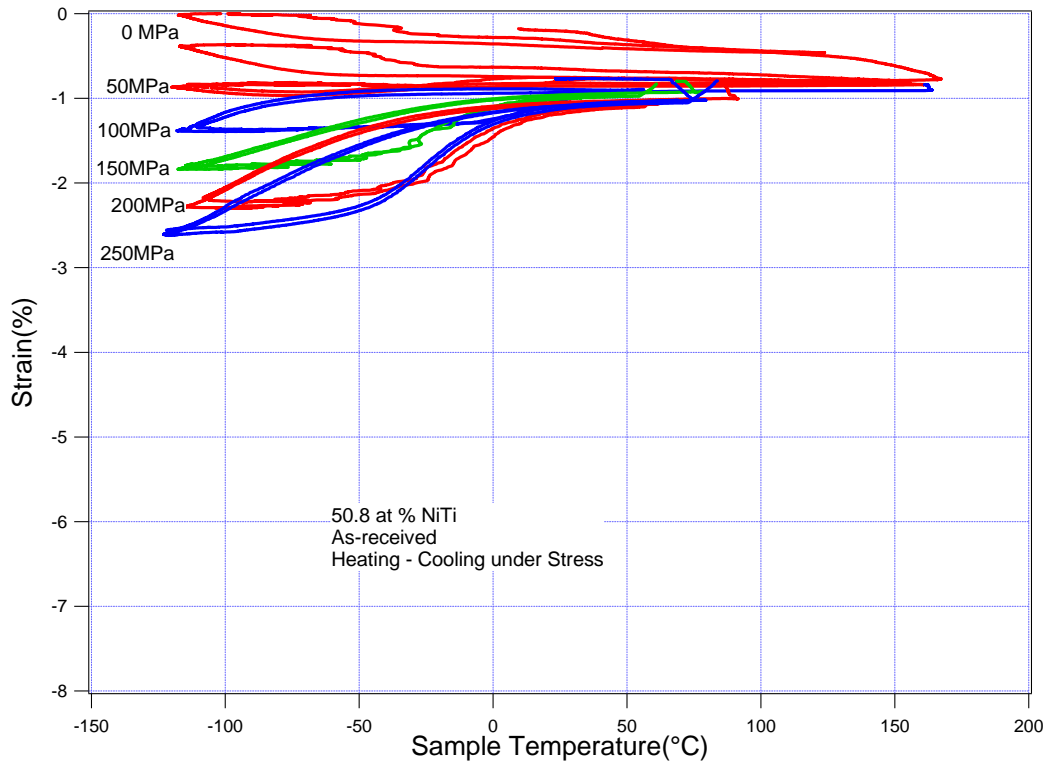


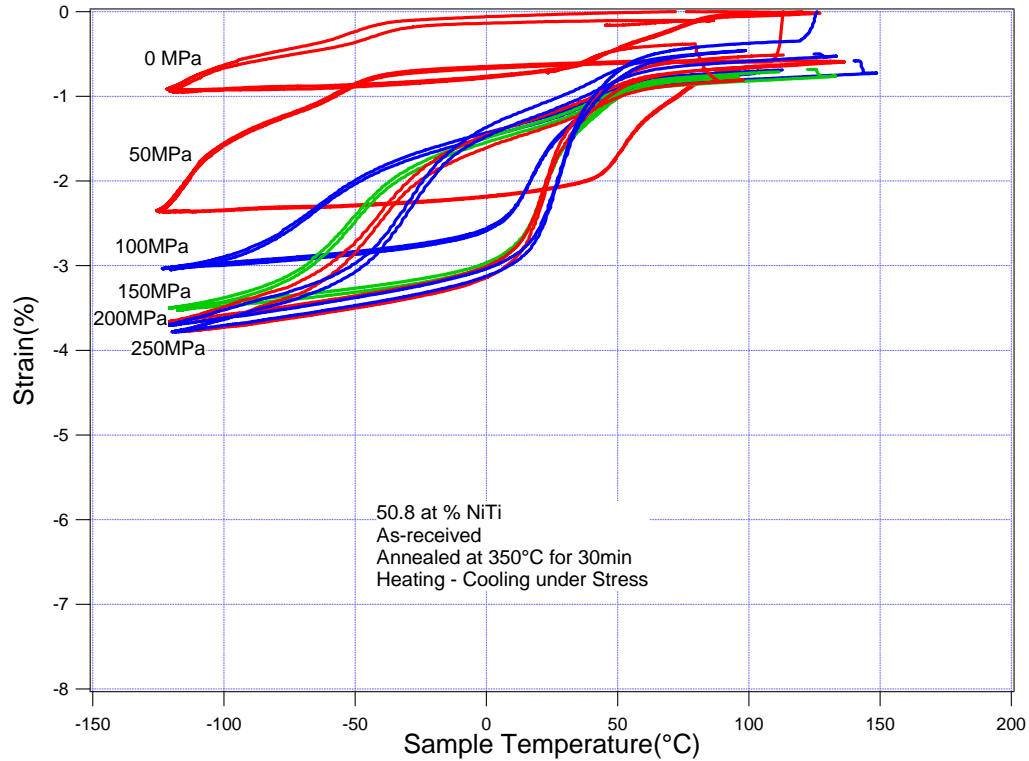
Figure 4.4.2 Definition of transformation strain and thermal hysteresis on a standard strain - temperature response of SMAs during thermal cycling under stress.

Figures 4.4.3 (a-f) show typical strain - temperature response for various deformation and heat treatment conditions during these experiments. Since no pseudoelasticity was observed in the solutionized material after the 450°C – 1hr heat treatment (Figure 4.4.1.d), a 400°C – 30 min heat treatment was used instead for these experiments.

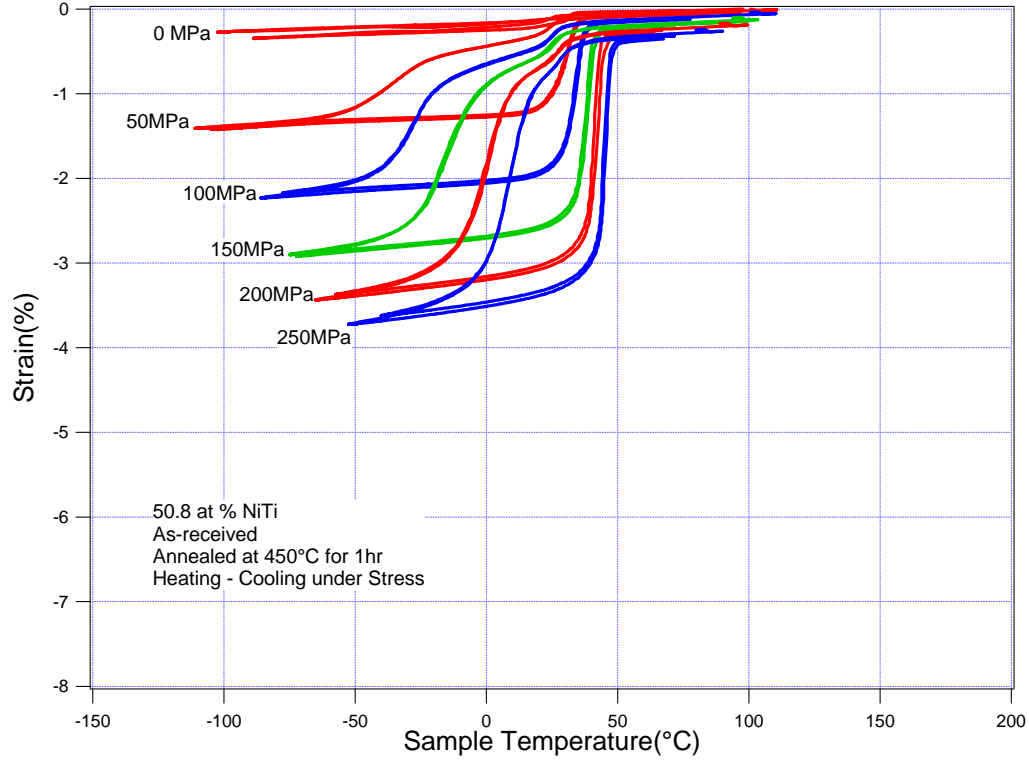


(a)

Figure 4.4.3 Strain - Temperature response under thermal cycling at various stress levels for (a) as-received, (b) as-received + annealed at 350°C for 30min, (c) as-received + annealed at 450°C for one hr, (d) solutionized, (e) solutionized + aged at 400°C for 30min, and (f) ECAE processed at 450°C.

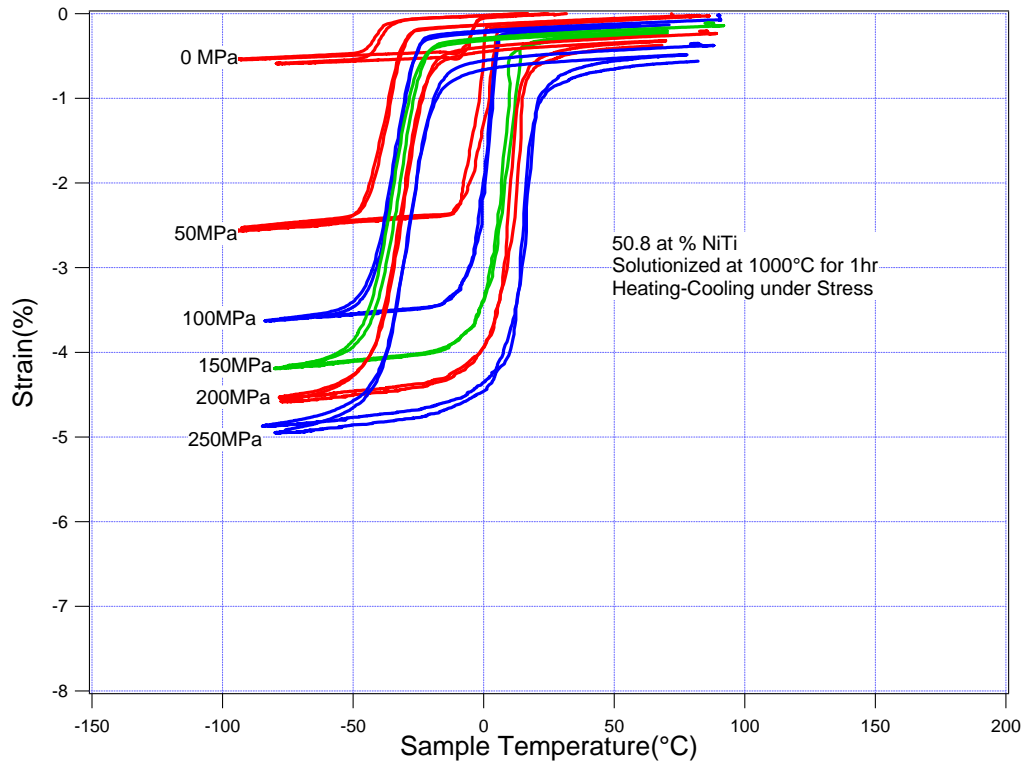


(b)

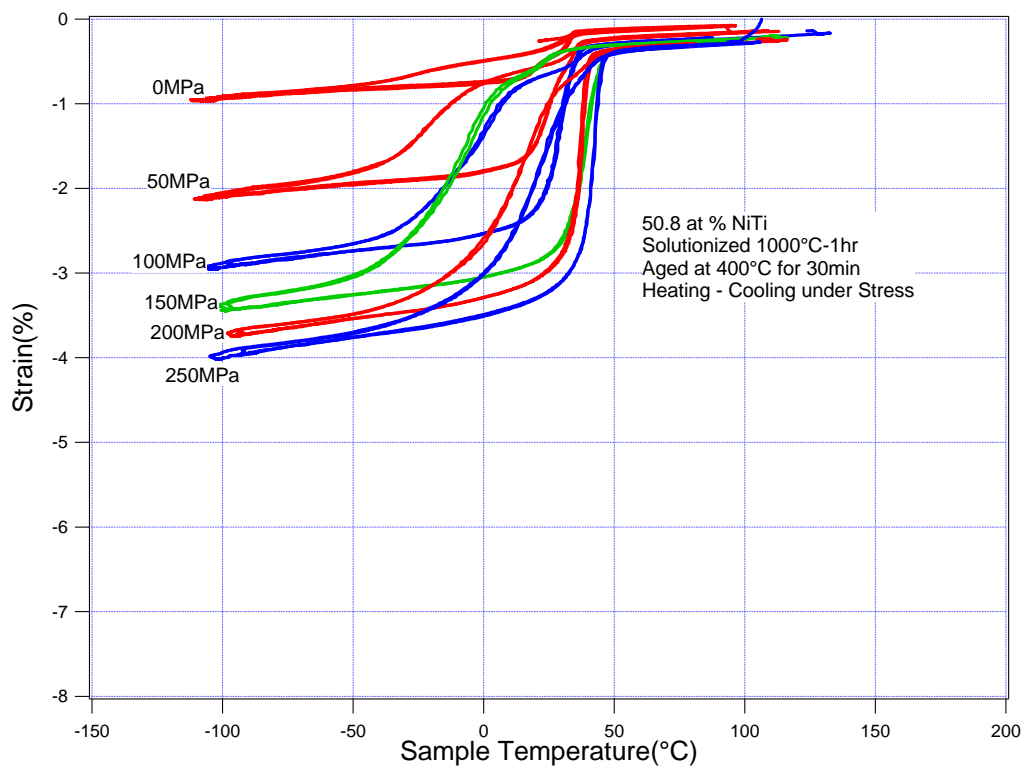


(c)

Figure 4.4.3 Continued.

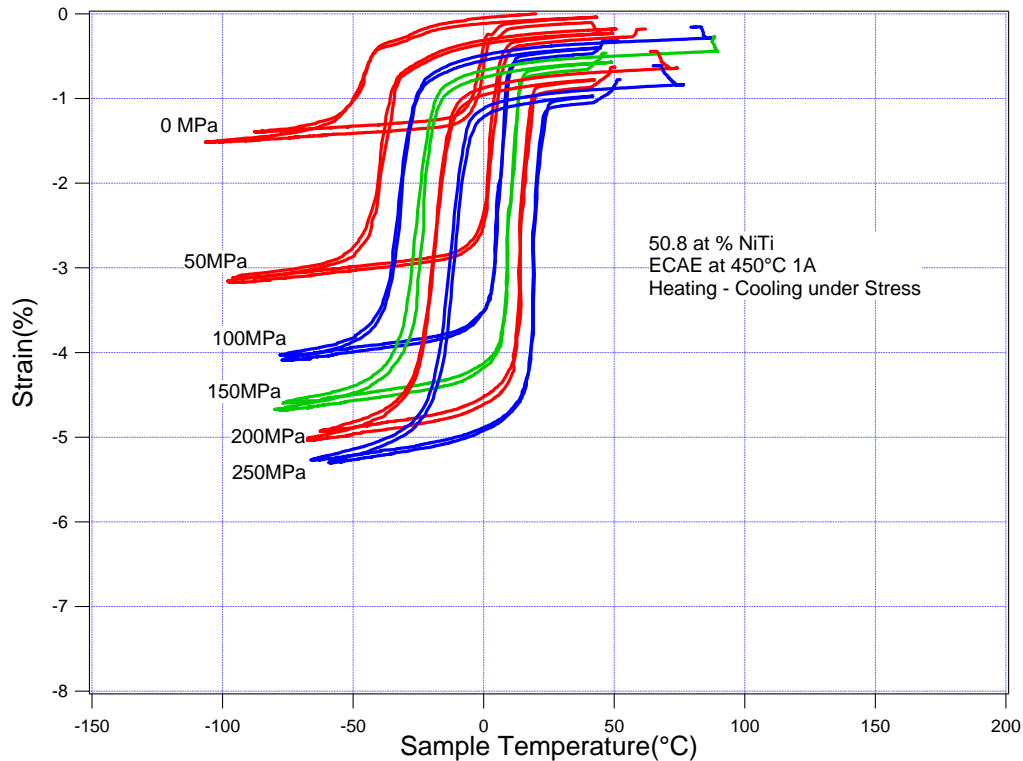


(d)



(e)

Figure 4.4.3 Continued.



(f)

Figure 4.4.3 Continued.

Figure 4.4.4 shows the variation of transformation strain as a function of applied stress for various deformation and heat treatment conditions. The transformation strain increases with applied stress for all of the deformation and heat treatment conditions due to an increase in the volume fraction of favorably oriented martensite variants at the expense of other unfavorably oriented variants [48]. The as-received material before and after annealing shows very low values of transformation strain due to the dislocation structure acting as a barrier to the austenite-martensite interface motion. For the ECAE processed material, there is dynamic recovery and recrystallization occurring at 450°C [31,32] which preserves the transformability while strengthening the alloy. Usually, very low transformation strains are experienced under zero load conditions because martensite variants form a self accommodating structure resulting in zero displacement [48], but the

ECAE processed material shows considerable transformation strain (1.35%) at 0 MPa. This seems to imply that during ECAE processing, a specific texture might have evolved or there might be internal residual stress which bias the growth of a single martensite variant.

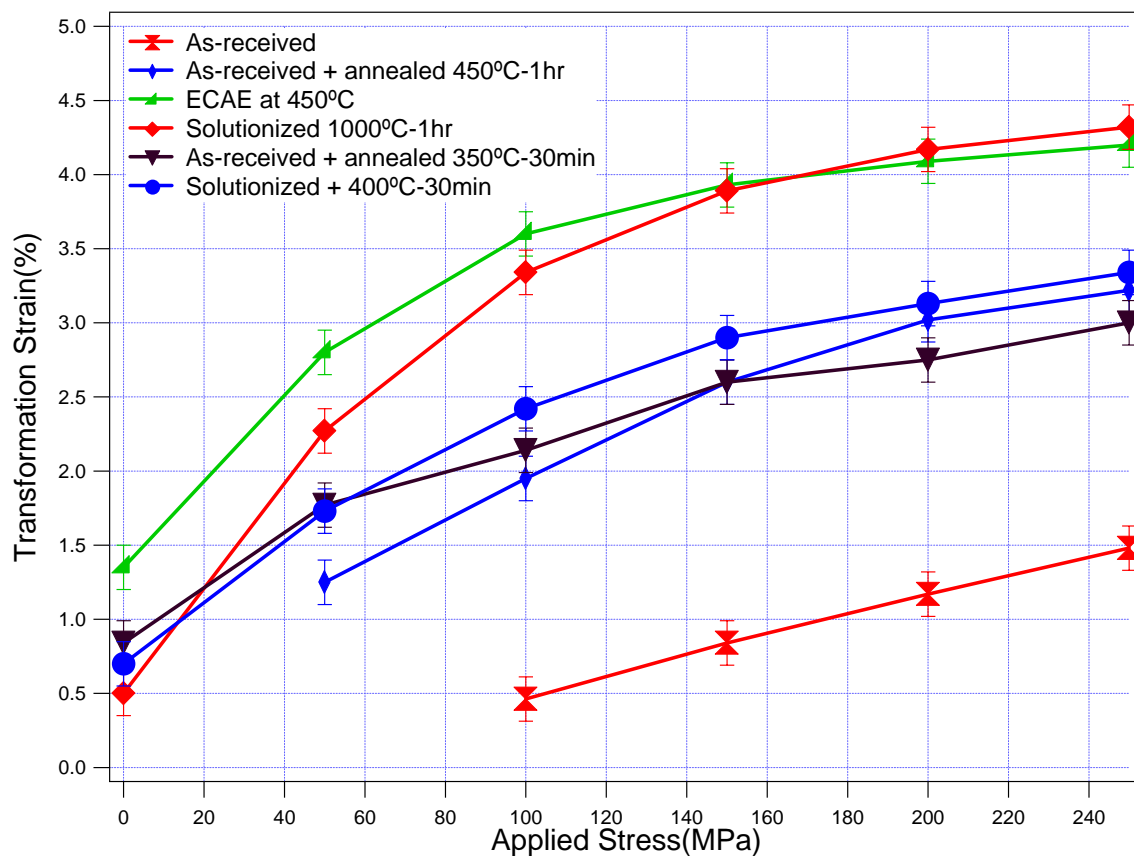


Figure 4.4.4 Variation of transformation strain as a function of applied stress for various deformation and heat treatment conditions.

Figure 4.4.5 shows the stress dependence of thermal hysteresis for various deformation and heat treatment conditions. Considerable overheating is required for the as-received material to annihilate the dislocations and overcome the barrier to interface

motion which explains the exceptionally high hysteresis. The solutionized material shows an expected increase in hysteresis as a function of stress indicating an increase in dissipation energy due to the formation of dislocations during cycling. The as-received material after annealing and the ECAE processed material showed an unusual decrease in hysteresis with stress, but the absolute values of the hysteresis for the ECAE processed material are lower than than for the as-received material after annealing at all stress levels. Thus the ECAE material sample shows the most promising results for stable cyclic response under thermal cycling.

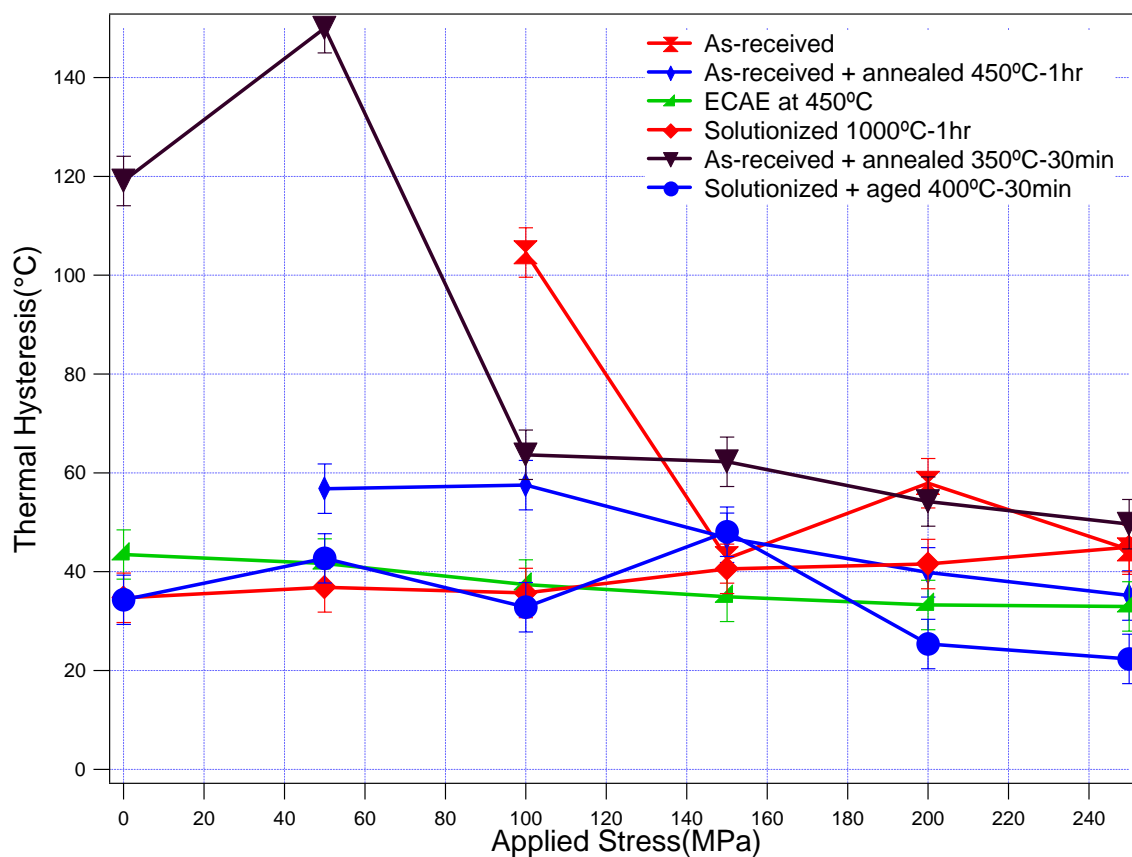


Figure 4.4.5 Stress dependence of thermal hysteresis for various deformation and heat treatment conditions.

Figure 4.4.6 shows the variation of irrecoverable strain as a function of applied stress for various deformation and heat treatment conditions. The as received material before and after low temperature annealing treatment shows very low values of irrecoverable strain at all stress levels. The same is true for the aged material which showed 0% irrecoverable strains at all stress levels. But the ECAE at 450°C sample showed relatively high values of irrecoverable strain which could be attributed to recovery and grain growth occurring during ECAE processing. The solutionized material shows very poor response under thermal cycling with a continuous increase in irrecoverable strain as a function of stress due to formation of defects at the austenite/martensite interface.

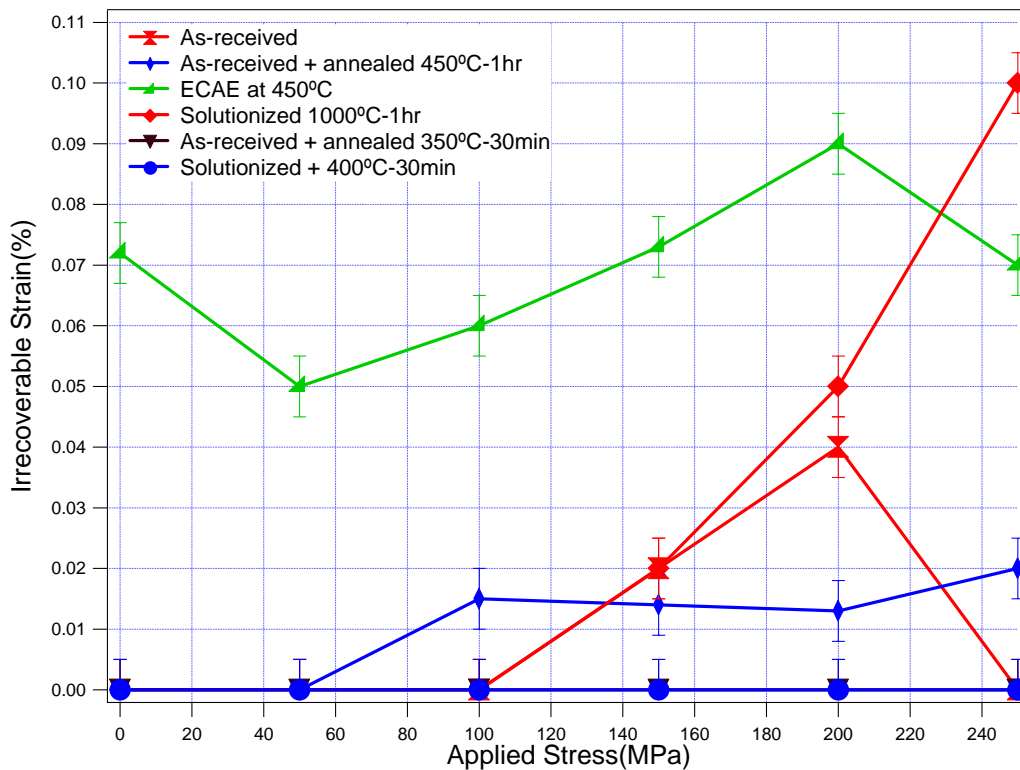


Figure 4.4.6 Variation of irrecoverable strain as a function of applied stress for various deformation and heat treatment conditions.

c. Pseudoelastic cyclic response

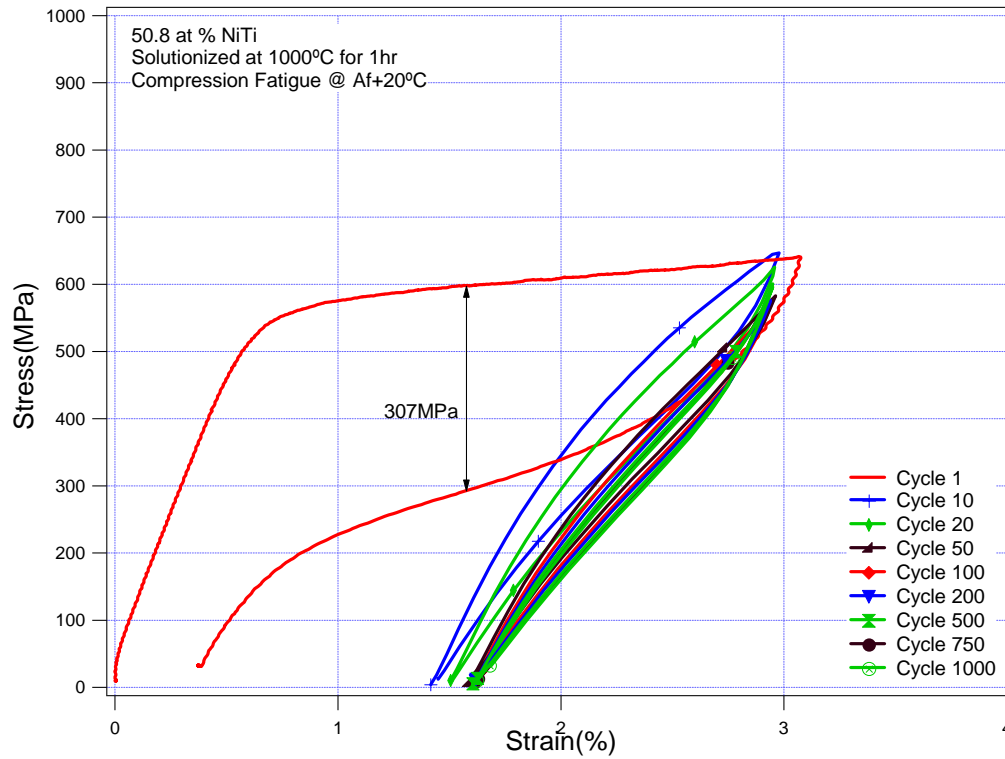
Figure 4.4.7 shows the pseudoelastic cyclic response under 3% compressive strain at $A_f + 20^\circ\text{C}$ for 1000 cycles for (a) solutionized material, (b) as-received and annealed at 450°C for one hr and (c) ECAE processed at 450°C . Only selected cycles are shown after regular intervals for convenience and ease of understanding. The reason for conducting experiments at $A_f + 20^\circ\text{C}$ is explained in Section 4.4 (a). The main goal of these experiments is to observe the effect of mechanical cycling on recoverable strain and stress hysteresis for different deformation and heat treatment conditions. No experiments are conducted on the as-received material because continuous hardening is observed in incremental strain loading experiments without a plateau region during transformation (Figure 4.4.1 (a)). Also, the sample solutionized and aged at 450°C for one hr shows irrecoverable strain of 2% out of 3% strain in compression in the first cycle (Figure 4.4.1 (d)) due to large incoherent precipitates which are unable to undergo transformation. Thus pseudoelasticity cyclic experiments were not conducted on these samples.

Figures 4.4.7 (a) and 4.4.7 (b) show the pseudoelastic cyclic response for the solutionized and the as-received material after annealing at 450°C for one hr, respectively. Both samples show very poor cyclic response with the maximum degradation occurring in the first 10-20 cycles. There is a total irrecoverable strain of 1.74% for the solutionized material and 1.64% for the as-received and annealed sample out of 3% applied strain after the 1000th cycle. This means less than 50% of the total transformation strain is recovered after the 1000th cycle in both cases. This is due to the residual stabilized martensite which is prevented from reverse (back to austenite) transformation by the dislocations generated during cycling [25]. There is considerable hardening with a decrease in transformation stress (stress for inducing martensite) and a dramatic change in the stress hysteresis of the samples. Moreover, as the cycling proceeds, hardening, transformation stress, stress hysteresis and irrecoverable/plastic strain reach saturation producing fully reversible transformation. This decrease in transformation stress level, hardening and the drastic change in stress hysteresis can be explained by the cyclic dislocation generation especially in soft materials and by residual martensite. When the stress is applied, initially the residual martensite/austenite interface moves resulting in a lower stress level for SIM. But this motion is difficult, so there is a

high hardening probably until significant nucleation and growth of new martensite crystals occurs at a higher stress level. Dislocation structures formed during cycling can trigger the nucleation of new martensite crystals at a stress level lower than that for the previous cycle due to their surrounding stress fields. Thus, as the dislocation density increases the transformation stress decreases.

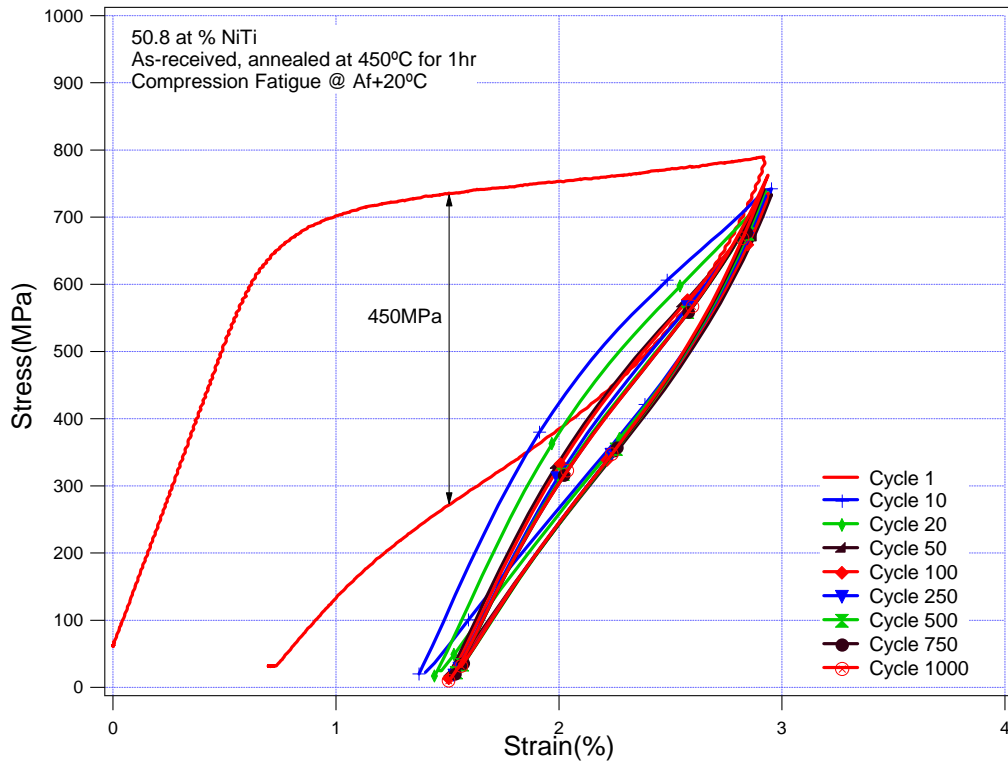
Figure 4.4.7 (c) shows the pseudoelastic response of the ECAE processed material, showing an outstanding improvement in the cyclic response of the alloy. 100% strain was recovered up to the 1000th cycle with 0% residual or irrecoverable strain. Also, there is comparatively less hardening and a small change in the hysteresis/cyclic loop shape as compared to the solutionized material and the as-received material after annealing. This improvement in cyclic response is due to strengthening via microstructural refinement and probably due to the formation of specific texture. During ECAE processing, dislocations are introduced into the matrix of the parent phase which in turn prohibits nucleation of new defects during cycling and thus enhances the cyclic stability.

The stress hysteresis values for the solutionized and the as-received materials after annealing (Figure 4.4.7 (a), 307 MPa and Figure 4.4.7 (b), 450 MPa, respectively) are higher than for the ECAE processed material (Figure 4.4.7 (c), 216 MPa). This stress hysteresis is caused by lattice resistance to the austenite-martensite interface motion and by dissipation. Thus, a lower value of stress hysteresis is an indication of stable cyclic response due to less dissipation.

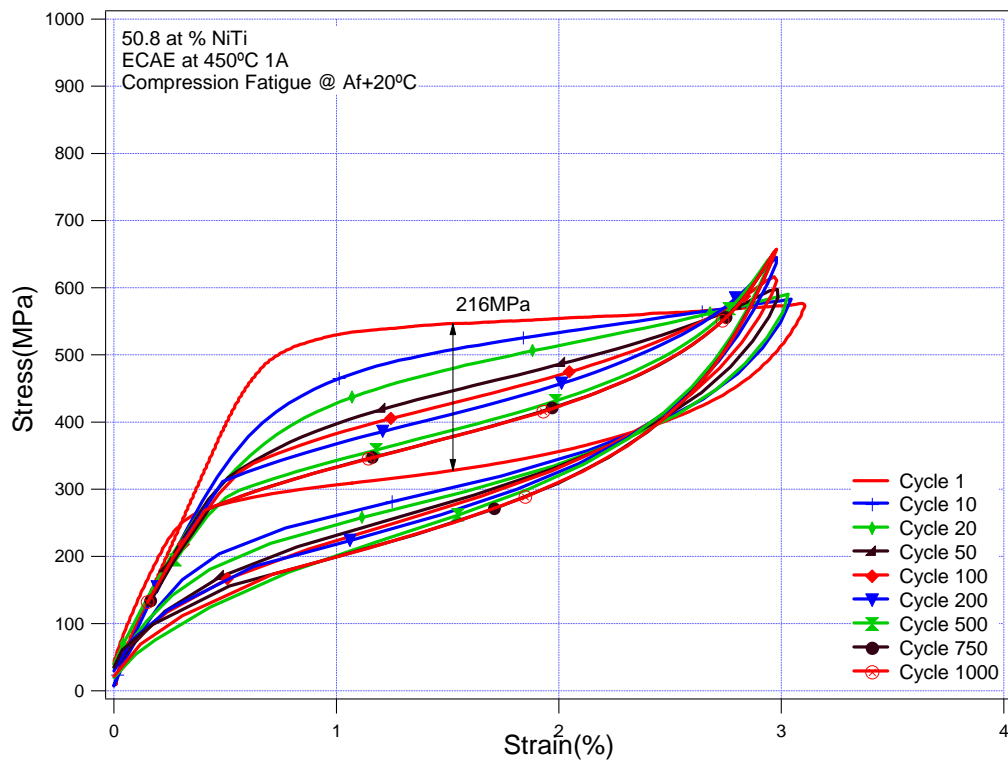


(a)

Figure 4.4.7 Cyclic response at 3% compressive strain for (a) solutionized, (b) as-received, annealed at 450°C for one hr and (c) ECAE at 450°C.



(b)



(c)

Figure 4.4.7 Continued.

Table 4.4.1 summarizes important parameters pertinent to cyclic response of shape memory alloys for all the deformation and heat treatment conditions.

Table 4.4.1 Comparison of various parameters pertinent to cyclic response of shape memory alloys for different deformation and heat treatment conditions, SIM: Stress for Inducing Martensite, PE: Pseudoelastic.

Sample	Incremental Strain loading				Heating Cooling under Stress		Fatigue cycling to 1000 cycles at 3% Strain	
	Yield Stress(MPa) B	SIM (MPa) A	A/B	Max PE Recoverable Strain(%)	Transformation Strain(%) at 250MPa	Thermal Hysteresis at 250MPa	Irrecoverable Strain after 1000th cycle(%)	Stress Hysteresis at 1st Cycle (Mpa)
As-received				2	1.5	44		
As-received, Annealed 350C-30min					3	49.62		
As-received, Annealed 450C-1hr	1620	700	0.43	2.25	3.22	35	1.64	450
Solutionized	1010	500	0.49	3.34	4.3	45	1.74	307
Solutionized, Aged 400C-30min					3.34	22.34		
Solutionized, Aged 450C-1hr		550		1.44				
ECAE at 450C	1620	525	0.32	3.73	4.2	33	0	216
Requirement for stable cyclic response	Higher the better	Lower the better	Lower the better	Higher the better	Higher the better	Lower the better	Lower the better	Lower the better

d. Effect of ECAE on ductility

Figure 4.4.8 shows the incremental strain response under tension of 50.7 at % NiTi Hot Rolled material after ECAE at 450 °C 1A. 28.44 % elongation to failure was observed in the material, and this indicates that ductility is preserved after SPD using ECAE at elevated temperature (equivalent strain ~1.16 at each pass) in NiTi. The stress to failure is 967 MPa, and the stress for inducing martensite (SIM) is about 335 MPa. These values are very low as compared to the respective values under compression

(Table 4.4.1). This asymmetry is attributed to two factors. One factor is the difference at which the experiments were conducted ($A_f + 20\text{ }^\circ\text{C}$ under compression compared to A_f under tension). This additional $20\text{ }^\circ\text{C}$ temperature under compressive loading lead to an increase in the yield stress and SIM according to the Clausius-Clapeyron relationship [23]. According to the Clausius-Clapeyron relationship, the SIM and yield stress are directly proportional to the deformation temperature up to M_d (the highest temperature at which SIM is observed) after which it decreases since diffusion and grain boundary sliding are the main deformation mechanisms. The second factor is the asymmetry due to tensile and compressive loading where the values of critical resolved shear stress are lower in tension as compared to compression [36]. But the values of PE recoverable strain are higher under tension than compression (Figure 4.4.1 (e)) for the same deformation condition (ECAE at $450\text{ }^\circ\text{C}$ 1A). This asymmetry can be attributed to the values of detwinning strain under tension and compression. Typically these values are lower in compression than tension [36]. The stress plateau is perfectly flat as under tension whereas there is relative hardening under compression for the same deformation condition (ECAE at $450\text{ }^\circ\text{C}$ 1A, Figure 4.4.1 (e)). A possible explanation could be generation of defects during transformation under compressive loading.

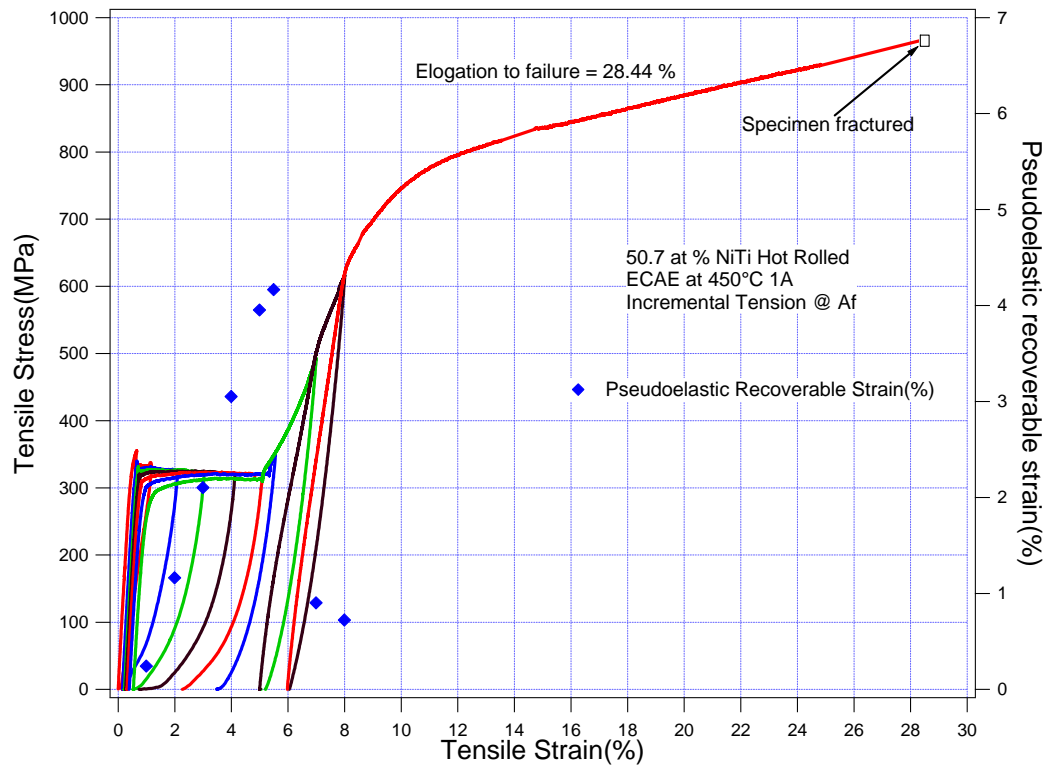


Figure 4.4.8 Incremental strain response under tension of 50.7 at % NiTi Hot Rolled material after ECAE at 450°C 1A.

CHAPTER V

CONCLUSION AND FUTURE RECOMMENDATION

In this study, a Ti-50.8 at% Ni alloy was severely deformed at room temperature and at 450 °C in the B2 austenite phase using Equal Channel Angular Extrusion (ECAE). Resulting transformation characteristics and microstructural evolution were investigated. It was found that in the samples ECAE processed at room temperature, austenite stabilization occurred after severe deformation although martensite stabilization was expected. The mechanism of austenite stabilization was attributed to the $B2 \xrightarrow{\text{SIM}} B19' \xrightarrow{\text{SPD}} B2$ (SIM: stress induced martensite, SPD: severe plastic deformation) transformation sequence. Upon low temperature annealing, highly organized, twin related nanograins formed with a size of about 100 nm in B2 austenite. The microstructural mechanism responsible for this structure was described as: 1) stress induced martensitic transformation in austenite and following heavy compound twinning in martensite, 2) accumulation of lattice dislocations along compound twin boundaries, and 3) back transformation of each martensite twin into an austenite nanograin with approximately exact theoretical lattice correspondence. The austenite nanograins formed where the martensite twins were due to the difficulty of moving the twin boundaries with high dislocation density even after low temperature annealing. These nanograins were twin related. In the samples ECAE processed at 450 °C, strain induced B19' martensite was observed which is unusual at such a high temperature. This methodology of utilizing SPD via ECAE and low temperature annealing may open a new opportunity for twinning induced grain boundary engineering in NiTi alloys. Thus ECAE processing leads to thermomechanical strengthening of the alloy via grain size refinement, formation of specific texture and introduction of dislocation structure while preserving the ductility. ECAE has advantages in terms of ease of processing, control on grain morphology, evolution of microstructure and formation of specific texture. ECAE processed material shows a stable cyclic response under thermal and pseudoelastic cycling making it a promising candidate for functional (one /two way shape memory effect) and structural (pseudoelastic displacement/damping) applications.

Future recommendation:

- Higher number of passes with different routes should be tried at different temperatures ranging from room temperature to 450 °C (50 °C, 100 °C, 150 °C... 400 °C).
- Texture analysis should be conducted to examine the effects of various routes on the texture evolution.
- Large diameter billets with large can size should be used for the ECAE extrusion.
- Extrusion should be conducted isothermally by incorporating appropriate changes in the tool design.

REFERENCES

1. Funakubo H. Shape Memory Alloys, Gordon & Breach Publishing Group, Amsterdam 1987; Page: 1.
2. Otsuka K, Wayman CM. Shape Memory Materials, Cambridge University Press, Cambridge 1998; Page: 1.
3. Murakami Y, Otsuka K. Mater Sci Eng A 1994; 189: 241.
4. Liu Y, Liu Y, Humbeeck JV. Acta Mater 1999; 47: 199.
5. Shaw JA, Kyriakides S. J Mech Phys Solids 1995; 43: 1243.
6. Sehitoglu H, Karaman I, Anderson R, Zhang X, Gall K, Maier HJ, Chumlyakov. Acta Mater 2000; 48: 3311.
7. www.ad.tut.fi/aci/courses/76527/Seminars2000/SMA.pdf (Accessed: 10.02.2003)
8. Mihalcz I. Per Pol Mech Eng 2001; 45: 75.
9. Wayman WM and Harrison JD. JOM-J Min Met Mat S 1989; 41: 26.
10. Duerig T, Pelton A and Stockel D. Mat Sci Eng A 1999; 273: 149.
11. Humbeeck JV. Mater Sci Eng A 1999; 273-275: 134.
12. Nishida M, Wayman CM, Honma T Metall Trans A 1986; 17: 1505.
13. Otsuka K and Ren XB. Intermettallics 1999; 7: 511.
14. Kudoh Y, Tokonami M, Miyazaki S, Otsuka K. Acta Metall 1985; 33: 2049.
15. Otsuka K, Ren X. Mater Sci & Eng A 1999; 273: 89.
16. Nam TH, Saburi T, Nakata Y, Shimizu KX. Met Trans 1990; 31: 1050.
17. Ren X, Otsuka K. Scripta Mater 1998; 38: 1669.
18. Miyazaki S, Otsuka K, ISIJ International 1989; 29: 389.
19. Sehitoglu H, Karaman I, Zhang X, Viswanath A, Chumlyakov Y, Maier HJ. Acta Mater 2001; 49: 3621.
20. Miyazaki S, Otsuka K, Wayman CM. Acta Metallurgica 1989; 137: 1873.
21. Hornbogen E. J. Mater. Sci. 2003; 38: 1.
22. Hornbogen E. J. Mater. Sci. 2004; 39: 385.
23. Hornbogen E, Mertinger V, Wurzel D. Scripta mater 2001; 44: 171.
24. Hosogi M, Okabe N, Sakuma T, Okita K. Materials Science Forum 2002; 394-395: 257.
25. Hurley J, Ortega AM, Lechniak J, Gall K, Maier HJ. Z. Metallkd. 2003; 94: 5.

26. Goldberg D, Xu Y, Murakami Y, Morito S, Otsuka K. *Scripta Metallurgica et Materialia* 1994; 30(10): 1349.
27. Miyazaki S, Imai T, Igo Y, Otsuka K. *Metall. Trans. A* 1968; 17:115.
28. Xie Z, Liu Y, Humbeeck J V. *Acta Mater* 1998; 46: 1989.
29. Moberly WJ, Proft JL, Duerig TW, Sinclair R. *Acta mater* 1990; 38(12): 2601.
30. Mertmann M, Bracke A, Hornbogen E. *Journal De Physique IV* 1995; 5: C8-1259.
31. Wurzel D. *Materials Science and Engineering A* 1999; 273–275: 634.
32. Treppmann D, Hornbogen D. *J Phys IV France* 1997; 7: C5-211.
33. Pushin VG, Stolyarov VV, Valiev RZ, Kourov NI, Kuranova NN, Prokofiev EA, Yurchenko LI. *Ann Chim Sci Mat* 2002; 27 (3): 77.
34. Sergueeva AV, Song C, Valiev RZ, Mukherjee AK. *Mater Sci Eng A* 2003; 339: 159.
35. Stolyarov VV, Zhu YT, Alexandrov IV, Lowe TC, Valiev RZ. *Mater Sci Eng A* 2003; 343: 43.
36. Gall K, Sehitoglu H, Chumlyakov YI, Kireeva IV. *Acta Mater* 1999; 47(4): 1203.
37. Karaman I, Karaca HE, Maier HJ, Luo ZP. *Metallurgical and Materials Transactions A* 2003; 34: 2527.
38. Segal VM, Hartwig KT, Goforth RE. *Mat. Sci Eng A* 1997; 224: 107.
39. Segal VM, Goforth RE, Hartwig KT. Texas A&M University, U.S. Patent No. 5,400,633, 1995.
40. Dlouhy A, Khalil-Allafi J, Eggeler G. *Phil Mag* 2003; 83: 339.
41. Sehitoglu H, Karaman I, Anderson R, Zhang XY, Gall K, Maier HJ, Chumlyakov YI. *Acta Mater* 2000; 48: 3311.
42. Larche FC. *Dislocations in Solids* (Amsterdam: North-Holland) 1979; 4: 135.
43. Kreye H. *Z Metallk* 1970; 61: 108.
44. Ardell AJ. *Acta Metall* 1972; 20: 601.
45. Cottrell AH, Bilby BA. *Proc R Soc Lond* 1949; A62: 49.
46. Harper S. *Phys Rev* 1951; 83: 709.
47. Ham FS. *J Appl Phys* 1959; 30: 915.
48. Hamilton R F, Sehitoglu H, Chumlyakov Y, Maier H J. *Acta Mater* 2004; 52:3383.

VITA

Ajay Kulkarni, son of Vinayak and Vrushali Kulkarni and elder brother of Aboli Kulkarni, was born in Pune, India in 1979. He graduated from Pune University, Department of Mechanical Engineering, in May 2001. He worked in an automobile manufacturing company in India, TATA Motors from Aug 2001 to June 2002. In Fall 2002, he enrolled in Texas A&M University to pursue a master's degree in the Department of Mechanical Engineering. He completed his research and received a Master of Science majoring in Mechanical Engineering in December of 2004. Following graduation, Ajay will seek a full-time job in the field of engineering. During his study, he was a co-author of one journal and author of two conference publications. His permanent address is:

5-Amol Near Paya Society,

Aundh, Pune 411007,

India

Phone: 91-20-25890805